HAL
open science

Coherent Satellite Monitoring of the Water Cycle Over the Amazon. Part 1: Methodology and Initial Evaluation

Victor Pellet, Filipe Aires, Dai Yamazaki, Fabrice Papa

To cite this version:

Victor Pellet, Filipe Aires, Dai Yamazaki, Fabrice Papa. Coherent Satellite Monitoring of the Water Cycle Over the Amazon. Part 1: Methodology and Initial Evaluation. Water Resources Research, 2021, 57, 10.1029/2020WR028647 . insu-03671342

HAL Id: insu-03671342

https://insu.hal.science/insu-03671342v1

Submitted on 24 Jun 2022

HAL is a multi-disciplinary open access archive for the deposit and dissemination of scientific research documents, whether they are published or not. The documents may come from teaching and research institutions in France or abroad, or from public or private research centers.

L'archive ouverte pluridisciplinaire **HAL**, est destinée au dépôt et à la diffusion de documents scientifiques de niveau recherche, publiés ou non, émanant des établissements d'enseignement et de recherche français ou étrangers, des laboratoires publics ou privés.

Copyright

Check for updates

AGU ADVANCING EARTH AND SPACE SCIENCE

Water Resources Research

RESEARCH ARTICLE

10.1029/2020WR028647

Coherent Satellite Monitoring of the Water Cycle Over the Amazon. Part 1: Methodology and Initial Evaluation

Victor Pellet[1,3], Filipe Aires[2,3], Dai Yamazaki[1], and Fabrice Papa[4,5]

[1]Institute of Industrial Science, The University of Tokyo, Tokyo, Japan, [2]ESTELLUS, Paris, France, [3]LERMA, Observatoire de Paris, Paris, France, [4]LEGOS, Toulouse, France, [5]Institute of Geosciences, Universidade de Brasilia, Brasilia, Brazil

Key Points:

- A satellite-data integration technique can exploit the water budget closure and water exchange between the sub-basins
- Satellite-based precipitation data set is improved compared to in situ gauges
- The evapotranspiration estimates are improved by stressing the water or energy limitation regime over the amazon

Correspondence to:

P. Victor,
vpellet@iis.u-tokyo.ac.jp

Citation:

Victor, P., Aires, F., Yamazaki, D., & Papa, F. (2021). Coherent satellite monitoring of the water cycle over the Amazon. Part 1: Methodology and initial evaluation. *Water Resources Research*, *57*, e2020WR028647. https://doi.org/10.1029/2020WR028647

Received 21 AUG 2020
Accepted 20 APR 2021

Abstract Monitoring coherently the Amazon Water Cycle (WC) using satellite observations is crucial for climate and water resources studies. The SAtellite Water Cycle (SAWC) integration methodology is introduced to optimize the satellite datasets. In this paper, the WC budget is balanced simultaneously over 10 sub-basins by constraining the horizontal water exchanges between them. Compared to an actual assimilation analysis, SAWC benefits from the use of water storage observations from Gravity Recovery and Climate Experiment. SAWC corrects the satellite evapotranspiration datasets that tend to under-estimate the water-limited evaporation over the central Amazon and to over-estimate the energy-limited evaporation over the northern Amazon. The SAWC precipitation estimates are evaluated against gauge measurements and show good overall results with a correlation varying from 0.94 to 0.99 and root-mean-square deviation between 16 and 41 mm/month (≃10% of precipitation estimate).

Plain Language Summary The Amazon basin is the major hydrological basin on Earth, but quantifying its various water stocks and fluxes by using satellite observation remains a true challenge. In order to obtain a better description of the water cycle, we propose here a new methodology that optimizes all the available satellite estimations. Compared to previous efforts, river discharge measurements are used to constrain the horizontal water exchanges among the sub-basins. This methodology allows obtaining a more accurate and coherent quantification of the water cycle, at the regional scale. The optimized rainfall estimates show improvement compared to original datasets when evaluated against gauge measurements. The methodology corrects also the evapotranspiration season estimate that tends to under-estimate the water-limited evaporation over the central Amazon and to over-estimate the energy-limited evaporation over the northern Amazon.

1. Introduction

The Amazon is the largest drainage basin on Earth, with a total area of 6.10^6 km^2 (excluding Tocantins basin), and supplies 15%–20% of global freshwater input to the ocean. The average discharge at the most downstream gauging station Obidos is $\simeq 120 \cdot 10^3$ m$^3 \cdot$s^{-1} in December to $\simeq 300 \cdot 10^3$ $m^3 \cdot$s^{-1} in May (Moura et al., 2016; Ward et al., 2015) while the Tapajós and Xingu tributaries contributed an additional $17 \cdot 10^3$m^{3}s^{-1} in average to the total discharge of the Amazon River downstream of Obidos.

The Amazon region is currently facing risks due to climate variability and change, as well as increased anthropogenic pressures (Marengo et al., 2018; Nobre et al., 2016). While the basin is impacted by climate variability (Chaudhari et al., 2019; Espinoza et al., 2011; Guimberteau et al., 2013; Marengo et al., 2011) for both drought and flood, deforestation (Barlow et al., 2016; Guimberteau et al., 2017), damming for hydropower (Latrubesse et al., 2017) increase the risk of hydrologic alterations. However, crucial water components such as evapotranspiration are not well understood in particular the limitation of its regime based on energy or water (Builes-Jaramillo & Poveda, 2018; Espinoza et al., 2019; Maeda et al., 2017). A comprehensive and detailed picture of the spatial and temporal variations in water flows and stocks is therefore not fully obtained. Such information is essential for climate studies in the context of climate variability and anthropogenic pressure.

Observations can be used to investigate the terrestrial water balance (i.e., quantifying water storage, fluxes, and their variations). *In situ* measurements are unfortunately too sparse and unevenly distributed to support a coherent WC analysis at a global scale (Sheffield et al., 2009). Satellite observations present an

© 2021. American Geophysical Union. All Rights Reserved.

Table 1
Comparison of the Literature About the WC Analysis Over the Amazon

Studies	Main objectives	Multiplicity inputs for	Scale of analysis	EO error analysis	WC optimization
Azarderakhsh et al. (2011)	WC variability	*P*, *E*	Basin & sub-basins	no	No
Rodell et al. (2011)	*E* estimate ion	*P*	sub-basin only	yes	No
Oliveira et al. (2014)	Trends estimateion	None	sub-basin only	yes	No
Moreira et al. (2019b)	Error estimateion	*P*, *E*	sub-basin only	yes	No
Builes-Jaramillo and Poveda (2018)					
Pan et al. (2012), Sahoo et al. (2011)	Budget closure	*P*, *E*, *dS*	Basin Only	yes	Yes
Abolafia-Rosenzweig et al. (2021); Zhang et al. (2018)					
Our study	Budget closure	*P*, *E*, *dS*	Basin & sub-basins	yes	Yes

Note. The column "Main objective" stresses the final goal of the study. The column "Multiple inputs" tells if several datasets have been used for describing precipitation P, evapotranspiration E or total water storage change dS. The column "Scale of analysis" tells if spatial averaging is done over the entire drainage area or multiple sub-basins. The column "EO error analysis" gives information on which studies focus on uncertainty estimation. The column "WC Optimization" indicates the studies where the WC budget is used as a constraint to optimize the water component estimates.

Abbreviation: WC, water cycle.

* EO stands for Earth Observations.

important opportunity for the estimation of WC components at various spatial and temporal resolutions, at the global scale, and over a long time span, particularly in regions with small numbers of *in situ* stations. The launch in 2002 of the Gravity Recovery and Climate Experiment (GRACE) enables estimation of total water storage change *dS* at a large scale, providing a new tool for water balance analysis (Tapley et al., 2004; Watkins et al., 2015). The upcoming Surface Water and Ocean Topography (SWOT) mission (Durand et al., 2010) uses a Ka-band wide-swath altimeter to provide information on the dynamic changes of height and extent of continental surface waters with a high spatial resolution (100 m). This mission will make it possible, for the first time on a global scale, to obtain detailed information on the dynamics of surface water stocks (such as rivers, lakes, and flooded areas).SWOT measurements may help our understanding of the Amazon hydrology, although sensing below dense vegetation will be challenging (Biancamaria et al., 2016). The GRACE Follow-On mission launched as GRACE-FO in 2018, the extension of the Tropical Rainfall Measuring Mission (TRMM) data record (Huffman et al., 2007) with the Global Precipitation Measurement mission, and the launch of the SWOT mission will provide comprehensive new observations for elucidating the WC.

Using satellite observations for WC monitoring is challenging due to the uncertainties associated with these estimates (systematic and random errors) and the inconsistency between datasets (for the same component or among components of the WC). Several studies have focused on the water conservation equation:

$$dS = P - E - R, \tag{1}$$

where *dS* is the total water storage change, *P* is precipitation, *E* is evapotranspiration, and *R* is discharged (expressed in mm/month, area-normalized). Table 1 provides information on various regional and global studies that have analyzed water balance based on satellite observations over the Amazon. If all studies of the water balance include observational data, various uses of the WC budget equation (i.e., water balance) are possible: (1) Most studies use the WC budget equation as a diagnostic tool for measuring the estimate's coherence. For example, Moreira et al. (2019b) investigated numerous combinations of satellite estimates, with uncertainties estimated using *in situ* data, to determine the water balance and identify the combination that best balances the surface WC budget. Builes-Jaramillo and Poveda (2018) jointly analyzed surface and atmospheric water balances over the Amazon for diagnosing discrepancy between various *E* estimates. (2) Some studies have used the WC budget directly to estimate one particular water component based on the three others at the basin scale: *E* (Maeda et al., 2017; Rodell et al., 2011), *R* (Abolafia-Rosenzweig et al., 2021; Azarderakhsh et al., 2011; Oliveira et al., 2014; Syed et al., 2005), and *dS* (Moreira et al., 2019b), to investigate trends (Oliveira et al., 2014) and seasonal patterns (Azarderakhsh et al., 2011; Moreira et al., 2019b).

(3) Finally, few studies have used the WC budget equation as a constraint for the optimization of satellite estimates for all water components. Pan and Wood (2006) developed an assimilation scheme in the Variable Infiltration Capacity (VIC) LSM at the basin scale. Extended this scheme to the pixel scale. Aires (2014) proposed several approaches, including a method to integrate various hydrological datasets with the WC budget closure constraint at the monthly scale without the use of surface or atmospheric models so that the obtained database is purely observational. Thus, suitable for model calibration and validation. Pellet et al. (2019) extended this methodology by requiring the water budget to be satisfied not only over land but also over the ocean and the atmosphere, and by constraining closure simultaneously at different spatial (entire Mediterranean area and regional drainage areas) and temporal (monthly and annual) scales.

In previous studies (Munier et al., 2014; Munier & Aires, 2018; Pan et al., 2012; Pellet et al., 2019, 2020), water budget optimization has been applied at the scale of an entire drainage basin. Therefore, only the spatial average over the entire basin was estimated. This approach cannot satisfy the fine-scale data requirements of many applications. Some developments have been made in downscaling the optimization from the basin scale to the pixel scale (Munier & Aires, 2018; Pellet et al., 2019). Sub-basins considerations are crucial when investigating large basins with multiple contrasting environments, such as the Amazon (Builes-Jaramillo & Poveda, 2018). For example, the seasonal peak rain signal can be delayed by up to two months in southern compared to northern regions, while mountainous regions (e.g., the Andes) do not show a monsoon precipitation pattern. Some sub-basins (e.g., the central region) are characterized by large wetland areas that impact the total water storage change dS locally (Alsdorf et al., 2001; Kim et al., 2009), and tropical forests in the western region are the main source of evapotranspiration for the entire basin Yang and Dominguez, (2019).

In this paper, we use the WC budget-based optimization framework developed previously (Aires, 2014) in imposing inter-basins constraints on the terrestrial budget closure based on consideration of horizontal water exchanges such as river discharge. This is a basic property of water flow that has not yet been used to optimize the satellite estimates of the water components (Aires, 2014; Pan et al., 2012; Pellet et al., 2019; Sahoo et al., 2011). The main innovation of the current paper is to explicitly use this information and *in situ* river discharges to better constraint the inter-dependent sub-basins. This new development allows better handling of various hydrological regimes that occur at the sub-basin scale throughout the Amazon basin. Our methodology, called SAtellite Water Cycle analysis (SAWC), represents well the WC and its local regimes in the largest river basin on Earth.

Section 2 introduces the study domain. Section 3 presents the datasets used in this study. The SAWC approach is described in Section 4. Section 5 presents the seasonality of the WC from our results. Section 5 includes our conclusions and some perspectives.

2. Study Domain

The Amazon region includes areas with various rainfall, evapotranspiration, and runoff patterns that vary spatially and seasonally (i.e., precipitation over the Andes, tropical monsoon). In this study, we divide the entire Amazon basin into 10 sub-basins Figure 1 (top).

These ten sub-basins have been selected based on the availability of *in situ* river discharge data from the SO-HYBAM (Amazon Basin Water Resources Observation Services, *https://hybam.obs − mip.fr/*). These sub-basins show various hydrological regimes, with precipitation peaks in different months. The sub-basins are chosen to be (1) small enough so that they do not mix several hydrological seasons, while (2) being large enough to allow the reduction of GRACE measurement errors by spatially averaging over the sub-basin area. The coarse resolution of the GRACE instrument limits the scale of the water budget analysis in imposing this trade-off. This has led to omitting few upstream stations of the HYBAM network.

The drainage areas were computed using a hydrological model (Wu et al., 2011) with a spatial resolution of 0.25°. 1-Tabatinga drainage basin is the most upstream sub-basin of the Amazon system. It includes part of the Andes Mountains and flows into 5-Manacapuru, which also includes part of the Andes in the northwestern part of the Amazon basin. 2-Porto Velho sub-basin is in the southern part of the Amazon basin and flows into 4-Fz. Vista. 3-Labrea drainage basin comprises the drainage of the Purus River, which

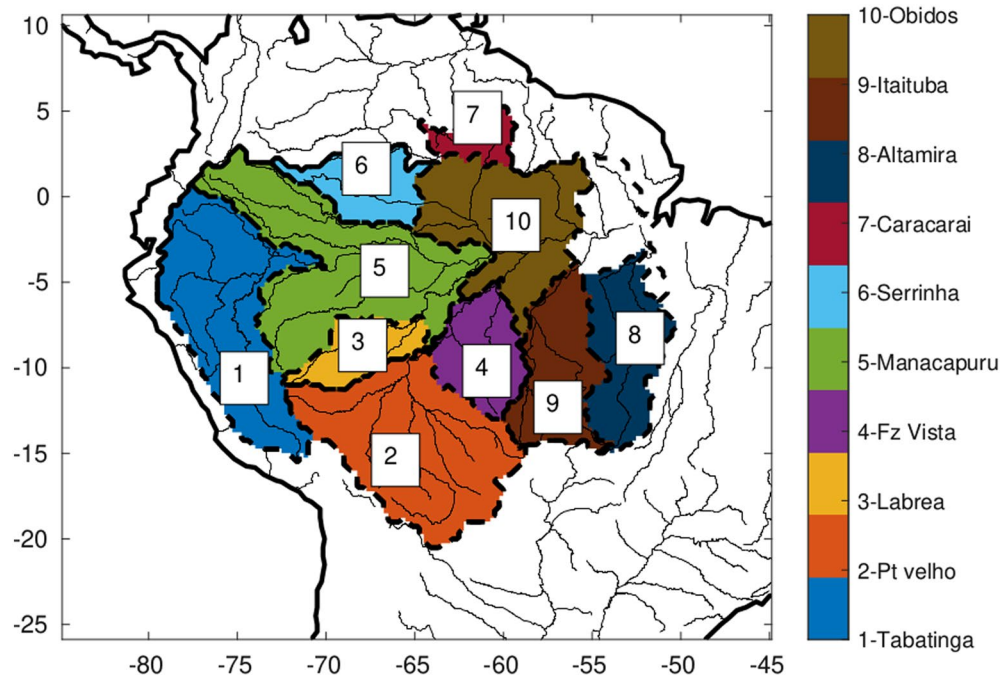

Figure 1. Amazon river drainage sub-basins are computed at 0.25° from a hydrological model (Wu et al., 2011). The most downstream station over the Amazon river is located in Obidos the basin outlet is then not included in the 10 sub-basins. Sub-basins are named by the location of the gauging station.

flows into 5-Manacapuru. 6-Serrinha and 7-Caracarai sub-basins carry water in the northern part of the Amazon basin. Along with 5-Manacapuru and 4-Fz. Vista, 6-Serrinha, and 7-Caracarai flow into 10-Obidos, the Amazon River. 5-Manacapuru and 10-Obidos are located in the rainforest part of the Amazon basin and have the largest inundated areas. 9-Itaituba and 8-Altamira are located in the eastern part of the Amazon drainage area and have lower rainfall variability due to their large drainage areas. A detailed description of these sub-basins can be found in (Azarderakhsh et al., 2011).

3. Datasets

This section describes all products used in this study. Table 3 provides additional information.

3.1. River Discharge

Monthly water discharge data are obtained from 10 gauge stations from the SO-HYBAM program. At these stations, SO-HYBAM provides accurate river discharge measurements, based on both observations of stages and water slope measurement which enable us to well represent looped rating curves (Callede et al., 2001, 2010; Paiva et al., 2013). Information about the location, the drainage area of sub-basins along with mean precipitation, mean discharge, and inundated areas can be found in Table 2.

3.2. Satellite Datasets

The datasets were used in the integration process to obtain an optimized estimation of the water components over the Amazon basin for which the hydrological coherency is enforced. Only global satellite products were considered. For integration, the datasets were projected onto a common grid with 0.25° spatial resolution based on the nearest neighbor interpolation and re-sampled at monthly intervals when necessary.

Table 2
Definition of the 10 Basins Considered in the articlnull Some of Their Hydrological Characteristic

Id	Station	Outlet location	River Name	Area (km^2)	P_{mean} mm/month)	R_{mean} ($\cdot 10^3$ m^3/s)	Inundated area (km^2)
1	Tabatinga	(-4.25°N; −69.93°E)	Amazonas	900,000	183	37,000	11,733
2	Porto Velho	(-8.74°N; −63.92°E)	Madeira	980,000	143	18,000	32,691
3	Labrea	(-7.25°N; −64.8°E)	Purus	230.000	176	5 700	119
4	Fz Vista Alegre	(-4.68°N; −60.03°E)	Madeira	340,000	182	27,000	2, 939
5	Manacapuru	(-3.31°N; −60.61°E)	Solimoes	1100,000	228	106,000	37,847
6	Serrinha	(-0.48°N; −64.83°E)	Negro	300,000	261	17,000	1 616
7	Caracarai	(1.83°N; −61.38°E)	Branco	130,000	167	3, 000	615
8	Altamira	(-3.38°N; −52.14°E)	Xingu	480,000	163	8, 000	1, 723
9	Itaituba	(-4.28°N; −55.58°E)	Tapajos	460,000	174	12,000	1, 894
10	Obidos	(-1.93°N; −55.5°E)	Amazon	730,000	208	181,000	73,968

Note. The sub-basins are the catchment defined in Fig. 1. All HYBAM river discharge measurements are available on the 1980–2015 time period.

3.2.1. Precipitation, *P*

The Tropical Rainfall Measuring Mission Multi-satellite Precipitation Analysis (TMPA, 3B42-V7) (Huffman et al., 2007) uses the Threshold Matched Precipitation Index algorithm to estimate instantaneous precipitation from multiple satellites. It merges TRMM microwave imager data with high-quality passive microwave observations from the Advanced Microwave Scanning Radiometer-Earth observing system (AMSR-E) and Advanced Microwave Sounding Unit in low-Earth observing orbit, as well as infrared data from a geosynchronous earth orbit. The version used here (3B42-V7) is obtained by combining satellite estimates with gauge measurements from the Global Precipitation Climatology Center (Schneider et al., 2011, 2014) using inverse random-error variance weighting of the gauge data. The TRMM data set extends from 50°N to 50°S with a spatial resolution of 0.25° and covers the period from January 1998 to the present (Huffman et al., 2007).

Multi-Source Weighted-Ensemble Precipitation (Beck et al., 2017) is a global dataset with a spatial resolution of 0.5° specifically designed for hydrological analysis (Beck et al., 2017). It merges the highest quality precipitation data sources available for each time point and location using a combination of rain gauge measurements, several satellite products including TMPA, and two reanalyses (ERA-Interim and JRA-55). Multi-Source Weighted-Ensemble Precipitation (MSWEP) data cover January 1979 to December 2016.

Several studies were dedicated to the evaluation of these datasets over different basins with various hydroclimatic conditions such as Huffman et al. (2007); Su et al. (2008) for TMPA and Beck et al. (2017, 2019); Liu et al. (2019) for MSWEP. Overall, these products compare well with rain gauge observations at the monthly time scale, even though large biases can affect daily rainfall amount estimates(Sun et al., 2018). The main improvement of these two datasets compared to others came from the incorporation of a daily rain-gauge correction (Beck, van Dijk, et al., 2017). Even if these datasets are not independent of each other, they represent the most up-to-date precipitation estimates available for hydrological studies. Moreira et al. (2019a) have compared these datasets, particularly over South America using 307 rain-gauge stations mainly located in the coastal region of Brazil (less than 30 are located in the Amazon basin). Over tropical regions, *P* satellite estimates based on infrared and microwave observations suffer from cloud coverage and signal saturation. Moreira et al. (2019a) provided a quantification of uncertainties and demonstrate that the MSWEP precipitation yielded a slightly lower uncertainty compared to TMPA while both vary up to 20%–40% in the Amazon basin. The authors also showed that uncertainties are site-specific while the uncertainty quantification itself relies on the availability of the *in situ* gauges.

3.2.2. Evapotranspiration, *E*

The Global Land Evaporation Amsterdam Model (GLEAM-V3B) (Martens et al., 2017; Miralles et al., 2011) uses an empirical energy-based equation (Priestley & Taylor, 1972) to calculate a reference evapotranspiration value, which is converted to actual *E* based on land cover and an evaporative stress factor. Separately,

Table 3
Overview of the Datasets Used in This Study

Dataset	Coverage	S. res. (°)	T. res.	Reference
Precipitation				
TMPA	1998–2017	0.25	Daily	Huffman et al. (2007)
MSWEP	1979–2017	0.25	Daily	Beck et al. (2017)
ERA-5	1980–2015	0.25	6h	Hersbach et al. (2020)
CDR	1984–2010	0.5	monthly	Zhang et al. (2018)
Gridded observation	1975–2009	0.5	Daily	Guimberteau et al. (2012)
Evapotranspiration				
GLEAM	1980–2017	0.25	Daily	Martens et al. (2017)
ERA-5	1980–2017	0.25	6h	Hersbach et al. (2020)
CSIRO	1981–2012	0.5	Monthly	Zhang et al. (2016)
CDR	1984–2010	0.5	Monthly	Zhang et al. (2018)
Water storage				
CSR	2002–2017	1	Monthly	Bettadpur (2012)
GFZ	2002–2017	1	Monthly	Dahle et al. (2013)
JPL	2002–2017	1	Monthly	Watkins and Yuan (2014)
MSC-JPL	2002–2017	0.5	Monthly	Watkins et al. (2015)
MSC-CSR	2002–2017	0.5	Monthly	Save et al. (2016)
CDR	1984–2010	0.5	Monthly	Zhang et al. (2018)
River discharge				
Observation	1980–2017	NA	Monthly	HYBAM
CDR-runoff	1984–2010	0.5	Monthly	Zhang et al. (2016)

Note. The WC budget is considered on the common coverage period 2002–2015.

Abbreviations: CDR, climate data record; CSIRO, Commonwealth Scientific and Industrial Research Organization; GLEAM, Global Land Evaporation Amsterdam Model; GFZ, German Research Centre for Geosciences; JPL, Jet Propulsion Laboratory.

this method estimates the components of land evaporation: transpiration, bare-soil evaporation, interception loss, open-water evaporation, and sublimation by considering four different types of land cover: bare soil, sparse vegetation, dense vegetation, and open water in each grid pixel. GLEAM uses reanalysis (vA) or satellite (vB) precipitation inputs to produce a daily data set at a spatial resolution of 0.25°.

The global observation-driven Penman-Monteith-Leuning (Zhang et al., 2016) evapotranspiration method is from the Commonwealth Scientific and Industrial Research Organisation (CSIRO). It uses the Penman-Monteith equations (Monteith, 1965; Penman, 1948), which account for both surface energy and atmospheric drivers. The satellite inputs are derived from the MODIS (Moderate Resolution Imaging Spectroradiometer) Global Evapotranspiration Project (Mu et al., 2011), and include land-cover classification, leaf area index, the fraction of photosynthetically active radiation, and albedo. CSIRO is a global data set at 0.5° resolution over the period 1980–2012.

These two datasets are considered satellite-based products even if their retrieval algorithms use auxiliary information and a model. We selected these two datasets due to their differing methods for calculating evapotranspiration. Inter-comparison of global evapotranspiration algorithms and datasets has been described previously (Michel et al., 2016). Validation of each data set against eddy flux tower observations can be found in (Miralles et al., 2011; Mu et al., 2011). Considering uncertainty, they are mainly a combination of the errors of the meteorological input data and the errors introduced by the (Priestley & Taylor, 1972) or (Monteith, 1965; Penman, 1948) models. Eddy flux towers network is very sparse in all the regions of the globe which limits the evaluation of the satellite estimates. Moreira et al. (2019a) have compared GLEAM

with MODIS-based datasets using 16 towers (mainly located in the southern Amazon basin) and calculated E uncertainty estimates at basin scale according to a land-cover classification. The authors provided an uncertainty of 22% (resp. 19) for MODIS-based (resp. GLEAM) over the Amazonian tropical forest. Over this region, E satellite estimates particularly suffer from the representation of the evapotranspiration over the seasonally flooded areas that are not taken into account in the models.

3.2.3. Total Water Storage Change, dS

All dS estimates are based on GRACE satellite measurements (Tapley et al., 2004). These estimates include surface water (wetlands, floodplains, lakes, rivers, and artificial reservoirs), soil moisture, snowpack, glaciers, and groundwater.

Three satellite datasets are available based on classical spherical harmonic (SH) decomposition of GRACE measurements: the Jet Propulsion Laboratory (JPL) (Watkins & Yuan, 2014) product; the Centre for Space Research (CSR) (Bettadpur, 2012) product, and the German Research Centre for Geoscience (Dahle et al., 2013) product. SH solutions solve monthly gravity anomalies (i.e., inter-satellite range-rate measurements) as water mass variations using truncated decomposition of the signal based on a spherical function. If the native resolution of GRACE estimate is around $3° \times 3°$, the SH products are provided at $1° \times 1°$.

Two solutions based on the mass concentration, known as MASCON, were also selected. The CSR-MSC solution is initially based on SH decomposition of the inter-satellite range-rate measurements and is then spatially truncated at the location of the mass concentration (Save et al., 2016). The JPL solution is based on an explicit estimation of mass anomalies at a specific equal-area mass concentration block location of $3° \times 3°$ using analytical partial derivatives of the inter-satellite range-rate signal (Watkins et al., 2015). The MASCON solutions are provided over a $0.5° \times 0.5°$ grid.

Two types of solutions were compared in terms of uncertainty in both min-max range and trend by Scanlon et al. (2016); Save et al. (2016). Scanlon et al. (2016) have shown the many advantages of the GRACE CSR and JPL mascon solutions relative to traditional SH solutions including reduced leakage perturbation, increased seasonal signal amplitude, and little or no postprocessing. Following the conclusive remarks in (Scanlon et al., 2016), we use both SH and MASCON solutions for S to indicates its uncertainty (Scanlon et al., 2016). For the SH solution, only the ensemble mean (simple arithmetic mean) of the three solutions is used (Sakumura et al., 2014) along with the two MASCON solutions.

3.3. ERA5 Reanalysis

In addition to Earth observations (EO), climate reanalysis datasets are also a good source of information, as they can provide coherent estimates for all water components. The European Centre for Medium-Range Weather Forecasts ERA5 (Hersbach et al., 2020) is used here as an alternative source for E and P. This fifth-generation reanalysis data set includes numerous improvements compared to ERA-Interim (Dee et al., 2011). The product has a global 0.25° resolution, considers the atmosphere to contain 137 levels from the surface to a height of 80 km, and covers the period of 1979–2019 at 6-h resolution. The atmospheric WC budget is balanced in the ERA5 reanalysis. Preliminary comparison through reanalysis of the land-surface parameter ERA5-Land showed that E does not differ significantly between ERA5 and ERA5-Land, so only ERA5 was used here.

3.4. Evaluation Datasets

3.4.1. Climate Data Record (CDR)

To evaluate the SAWC approach described in Section 4.1, we compared it to the P, E, dS, and R estimate from Zhang et al. (2018). This data set is referred to by Climate Data Record (CDR) in the following. Numerous products in the CDR have been optimally combined at 0.5° resolution for all water components using a weighted averaging technique (related to the ensemble spread and deviation from the ensemble mean). The authors then optimize these estimates using a constrained Kalman filter to ensure closure of the terrestrial water budget in each 0.5° grid cell (Zhang et al., 2018). For R values, only outputs simulated using VIC were used, and no *in situ* measurements were considered.

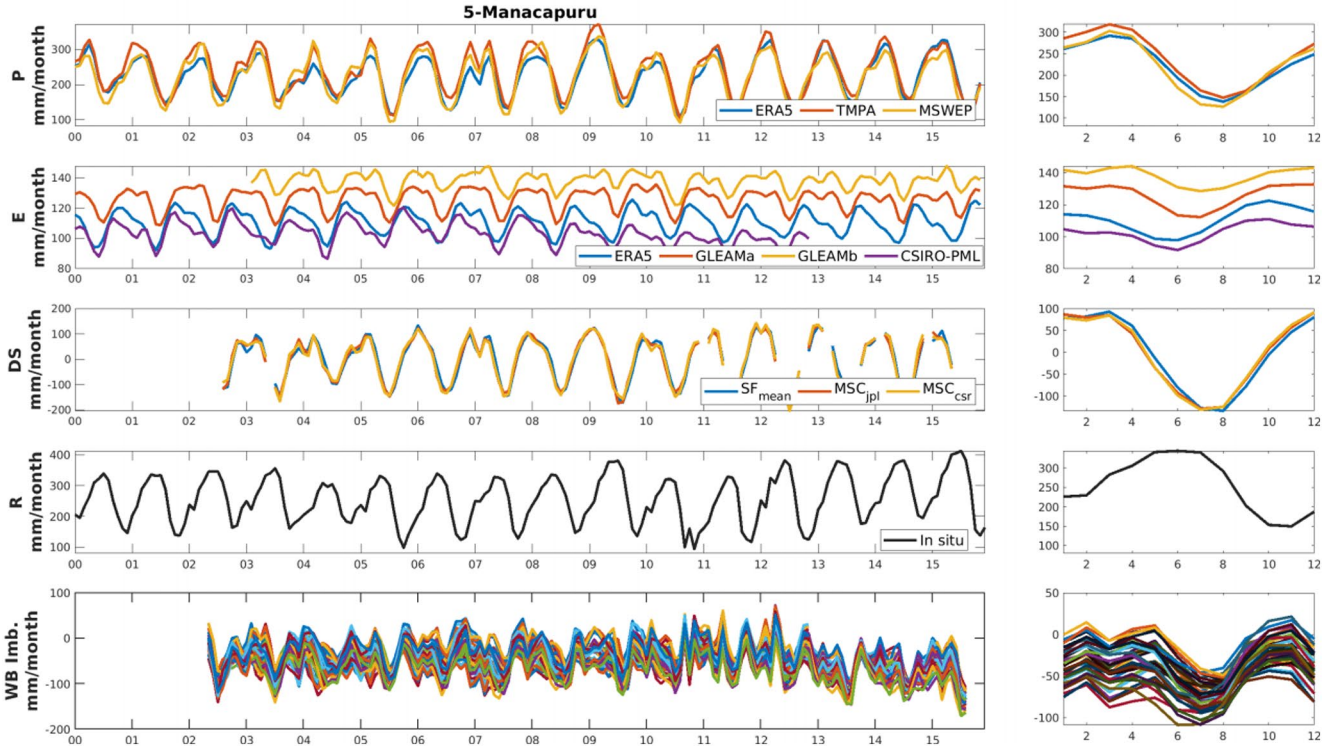

Figure 2. Representation of the datasets used in this study over the 5-Manacapuru sub-basin. From top to bottom, monthly variation (left) and climatology (right) for the four water components: precipitation *P*, evapotranspiration *E*, water storage change *dS,* and river discharge *R*. In each row, several datasets are used to depict the water component. The last row represents the resulting water budget imbalance (e.g., the residuals based on Equation 1) for all the (3 · 4 · 3 · 1) 36 possible combinations of singular dataset per water components. This last ensemble describes the overall water budget imbalance based on the various satellite estimates.

3.4.2. Gridded *In Situ* Precipitation *P*

Within the framework of the SO-HYBAM experiment, daily rainfall data from 1488 *in situ* gauges were gathered, covering the period from 1975 to 2009. After quality control (Espinoza Villar et al., 2009), ordinary kriging was performed to generate observation-based gridded daily rainfall data at a spatial resolution of 0.5° (Guimberteau, Drapeau, et al., 2012). The density of SO-HYBAM stations is about 125 [/10^6 km^2] over the Amazon basin, which is greater than that of the global gridded rainfall dataset for the Amazon. More information can be found in Guimberteau, Drapeau, et al., 2012).

4. SAtellite Water Cycle Assessment

The four first rows in Figure 2 show the times series (2000–2015) and seasonal climatology of all input estimates for each water component in the 5-Manacapuru sub-basin. All water components are described by numerous estimates that differ even at climatological scales (i.e., seasonally). Precipitation estimates are not independent of each other, as all include some information from gauges. Evapotranspiration shows the largest range of estimates compared to its range of observed variations. All *dS* estimates are based on GRACE satellite data and generally agree. The last row represents the residuals of the water budget (i.e., error with respect to Equation 1) for all the (3 · 4 · 3 · 1) 36 possible combinations of the EO datasets depicted in the upper panels of Figure 2 (one data set is chosen per water components). This last variable represents a diagnostic measure that can be applied to numerous estimates. The fewer the residuals are, the better the combination of EO is for depicting the water cycle. Based on these residuals, the WC budget is often used as a diagnostic tool for assessing the coherence of estimates. For this particular sub-basin, the imbalance ensemble shows a standard deviation (20 *mm/month*) lower than systematic bias (−40 *mm/month*) raising the issue in estimating accurately the mean value of *P* and *E* over the dense tropical forest.

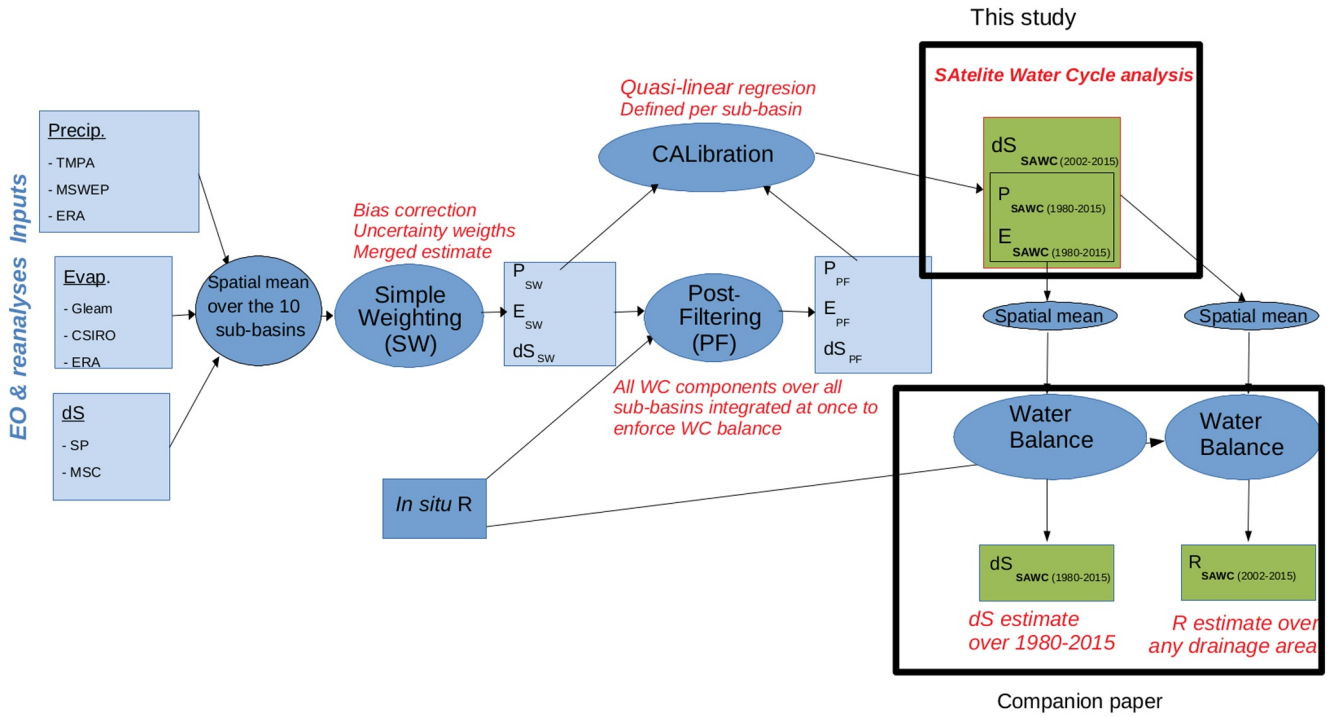

Figure 3. The SAWC processing steps: Simple Weighting in Section 4.2, the Post-Filtering in Section 4.3, the CALibration step in Section 4.4, and the optimized dataset obtained in this study are indicated with the "$_{sawc}$" subscript. In the companion paper, these SAWC products are used with the water balance to reconstruct (1) a *dS* estimate over a long period (1980–2015) and (2) a *R* estimate spatially distributed over the whole Amazon river system. SAWC, Satellite water cycle.

SAWC assessment provides a comprehensive description of the WC, which is obtained by optimizing the EO estimate while accounting for water budget closure. The WC budget is used not as a diagnostic tool, but instead as a constraint that must be satisfied. Figure 3 summarizes the main steps of the SAWC approach for meeting the objectives of this study and indicates the focus of our companion paper: the reconstruction of two water components, namely *dS* and *R*, using SAWC estimates. SAWC is based on (1) simple weighting (SW) merge of the various EO estimates of *P*, *E*, and *dS*; in this procedure, an *a priori* estimate and an uncertainty weight are obtained for those three components. (2) Integration for Post-Filtering (PF) the *a priori* estimates, which ensures closure of the WC in the sub-basins considered. Finally, (3) calibration is conducted based on quasi-linear regression, which allows approximation of the integrated solution from the *a priori* estimates without the use of all components over all sub-basins. This regression provides calibration among sub-basins. All of these steps have been introduced in previous studies (Aires, 2014; Munier et al., 2014; Pellet et al., 2019, 2020). The following sections describe the novel developments of this study that account for upstream/downstream dependency among sub-basins in the closure of the WC and briefly introduce the SW, PF, and calibration steps.

4.1. WC Budget Closure for Multiple Inter-Dependent Basins

This section is the core of the article. Optimization of the satellite estimates based on the closure of the water cycle has been introduced previously in the literature (Pan et al., 2012; Aires, 2014b; Munier et al., 2014; Pellet et al., 2019) but these efforts were applied only at the entire basin scale. This section describes how we account for the closure of the WC along river reaches that show upstream-downstream dependency. This new development is presented in the building of a constraint matrix G_{am} operating on a state vector X_{am}. Let $X_T^{'} = (P_T, E_T, R_T, dS_T)$ represent the state vector of the WC components over the drainage area (Aires, 2014). $'$ is the transpose sign and $_T$ is a subscript of "truth". The conservation of water mass at the basin scale can be considered a constraint on the state vector, expressed in Equation 2. A relaxed constraint is possible, as

shown previously (Pellet et al., 2019): the water budget is closed within an error r that follows a normal distribution with specified uncertainty (Yilmaz et al., 2011). The WC estimation task can thus be expressed as:

$$\begin{aligned} X_T^{'} &= (P_T, E_T, R_T, dS_T) \\ G &= [1, -1, -1, -1] \\ G \cdot X_T &= r \text{ with } r \sim \mathcal{N}(0, \sigma), \end{aligned} \tag{2}$$

where $^t G$ is the closure operator, and σ is the variance of the imbalance relaxation term r.

Following (Landerer et al., 2010; Pellet et al., 2020) and in order to avoid temporal mismatches between GRACE-derived dS and the monthly estimates of other water components, we used the centered difference of the mean TWS anomalies to compute $dS(t)$:

$$dS_t = \frac{S(t+1) - S(t-1)}{2}.$$

and to reduce the impact of this smoothing process on other water components when computing the WC budget, the following filter was applied:

$$Y = \frac{1}{4}Y(t-1) + \frac{1}{2}Y(t) + \frac{1}{4}Y(t+1)$$

where Y is P, E or R.

It is possible to consider multiple dependent sub-basins of affluent and confluent rivers flowing into the mainstream. The WC balance is constrained simultaneously over all sub-basins by considering water discharge that flows between sub-basins. Let us consider the global WC state vectors $X_{T,am}$ (dimension 40) of the 10 sub-basins:

$$X_{T,am}^t = [X_{T(1)}, X_{T(2)}, \ldots, \ldots, X_{T(10)}]. \tag{3}$$

which includes the four water components $X_{T,(i)}$ used in Equation 2 over each sub-basin i of area $A_{(i)}$.

For example, closure of the WC for the 5-Manacapuru sub-basin considers inflowing discharge from the 1-Tabatinga and 3-Labrea sub-basins and outflow to sub-basin 10-Obidos (in *mm/month* averaged over the 5-Manacapuru drainage area). This relationship can be described using the following dependent closure formula:

$$\begin{aligned} P_5 - E_5 - R_5 - dS_5 + \frac{A_{(1)}}{A_{(5)}}R_1 + \frac{A_{(2)}}{A_{(5)}}R_2 &= r \\ G \cdot X_{T(5)} + L_{5,1} \cdot X_{T(1)} + L_{5,3} \cdot X_{T(3)} &= r \end{aligned} \tag{4}$$

with:

$$L_{j,i} = \left[0\, 0\, \frac{A_l^{(i)}}{A_l^{(j)}}\, 0 \right] \tag{5}$$

The introduction of spatial dependency between sub-basins through the terms $L_{i,j} \cdot X_{(i)}$ is important for several reasons: (1) It improves the spatial scale of the integration by considering smaller and more hydrologically homogeneous sub-basins, (2) it accounts for available measurements of runoff routing between sub-basins, and (3) it potentially corrects downstream R observations with information from upstream discharge stations.

The water balance is then expressed as:

$$G_{am} \cdot X_{T,am} = (r\, r \cdots r)^t \sim \mathcal{N}(0, \Sigma), \tag{6}$$

where Σ is a 10×10 diagonal matrix. Notably, r may differ among sub-basins based on surface or underground (e.g., geological) characteristics. Here, we assumed that the water budget relaxation term r has similar characteristics for each sub-basin. The global "closure" matrix G_{am} becomes (10×40):

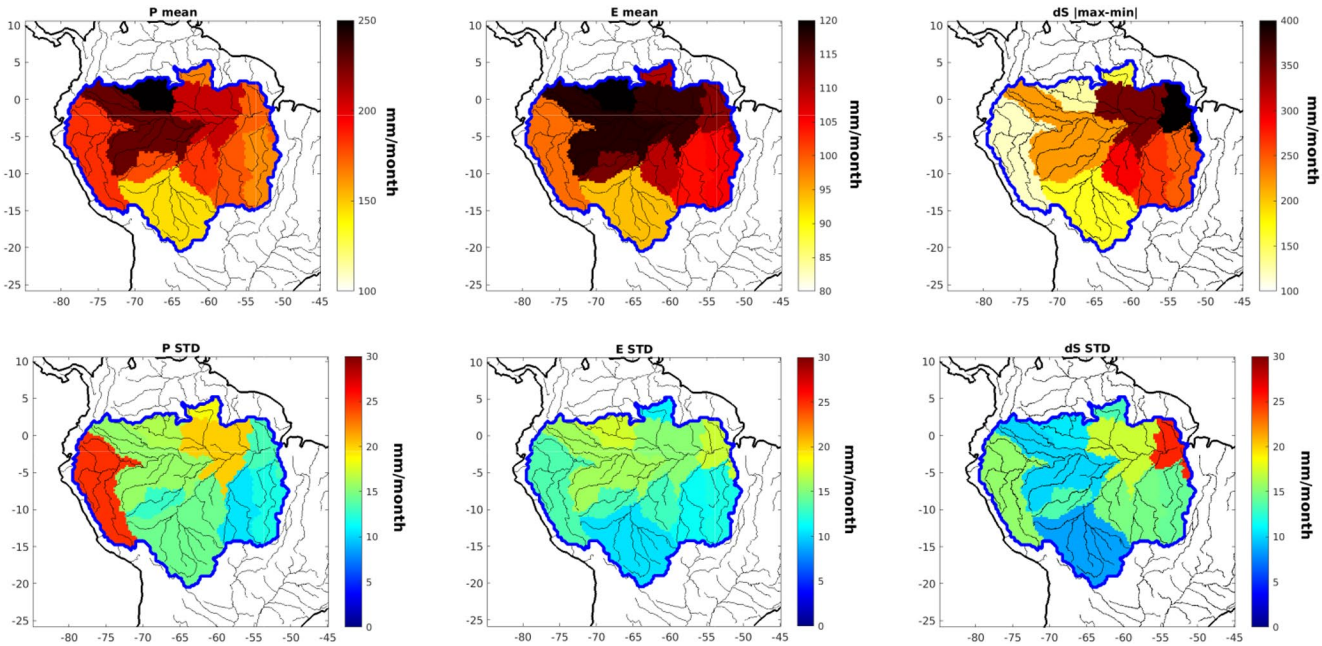

Figure 4. Representation of the *a priori* estimate. Annual mean (top) and its uncertainty (bottom) in mm/month for precipitation P_{SW} (left), evapotranspiration E_{SW} (middle), and total water storage change dS_{SW} (right), over the 10 sub-basins. The *a priori* estimate is computed from the Simple Weighting SW described in Section 4.2 while the associated uncertainty is defined as the spread of the input (satellite estimate) ensemble for each water component.

$$G_{am} = \begin{pmatrix} G & 0 & 0 & 0 & 0 & 0 & 0 & 0 & 0 & 0 \\ 0 & G & 0 & 0 & 0 & 0 & 0 & 0 & 0 & 0 \\ 0 & 0 & G & 0 & 0 & 0 & 0 & 0 & 0 & 0 \\ 0 & L_{4,2} & 0 & G & 0 & 0 & 0 & 0 & 0 & 0 \\ L_{5,1} & 0 & L_{5,2} & 0 & G & 0 & 0 & 0 & 0 & 0 \\ 0 & 0 & 0 & 0 & 0 & G & 0 & 0 & 0 & 0 \\ 0 & 0 & 0 & 0 & 0 & 0 & G & 0 & 0 & 0 \\ 0 & 0 & 0 & 0 & 0 & 0 & 0 & G & 0 & 0 \\ 0 & 0 & 0 & 0 & 0 & 0 & 0 & 0 & G & 0 \\ 0 & 0 & 0 & L_{10,4} & L_{10,5} & L_{10,6} & L_{10,7} & 0 & 0 & G \end{pmatrix} \tag{7}$$

The main novelty is the introduction of upstream-downstream dependency between sub-basins through the terms $L_{i,j}$ in matrix G_{am} along with the extended state vector $X_{T,am}$ (gathering all sub-basins). This shows how an *a priori* knowledge is transferred into a constraint matrix via the SAWC methodology.Following previous studies (Aires, 2014; Pellet et al., 2019), the relationship expressed in Equation 6 can be inverted to improve the *a priori* solution of the state vector.

4.2. *A Priori* Information and Associated Uncertainty

As shown in Figure 2, all water components can be described using the numerous estimates introduced in Section 3. These estimates are not consistent. The first step of integration is then merging them into an *a priori* (e.g., first guess) estimate which will be used further (Aires, 2014; Pellet et al., 2019). This step is called "simple weighting" (SW) since the resulting *a priori* estimate is based on the weighted average of all the inputs (e.g., satellite estimates) for one water component. When no information is available, the weight in SW is computed from the distance of each estimate from the mean (i.e., average). Three precipitation datasets are merged into one *a priori* estimate and similar approaches are used for the four E estimates and three dS estimates. Only one discharge data set was available so no merging is applied for R. We denote this *a priori* solution as $X_{SW} = (P_{SW}, E_{SW}, R, dS_{SW})$, where SW represents "simple weighting".

Figure 4 shows the long-term mean (top) of the *a priori* estimates for each water component throughout the Amazon basin. Precipitation is higher over the northern (6-Serrinha) and central (5-Manacapuru) regions of the basin, and evapotranspiration shows a similar pattern, with large transpiration from tropical forests. The variation of dS is greatest near the delta, where the amount of surface water associated with the river is the largest. For these three water components, discrepancies exist in the long-term mean between southern and northern sub-basins and the hydrological cycle appears to be more intense in the north (e.g., heavier rain, greater evapotranspiration, and larger changes in water storage). These local features can be observed only at the sub-basin scale with the northern and southern basins considered separately. If the entire basin had been considered instead, the average hydrological cycle would not have been representative of the southern region, where the water signal is relatively small.

Along with the *a priori* estimate of each water component, the associated uncertainties are required to characterize the quality of the *a priori* WC state. This information tells how trustful the *a priori* is and how far the constraint can modify it. Such characterizations are generally component- and site-specific. Following Pan et al. (2012); Sahoo et al. (2011); Zhang et al. (2018), the spread of the input ensemble (e.g., satellite estimate) can be used as a proxy for the uncertainty associated to the *a priori*. This method may lead to underestimation, as estimates might agree on an erroneous solution, but allows for coherent generic uncertainty estimation among water components. The *a priori* uncertainties for P, E, and dS are based on the spread among EO estimates, over each sub-basin. This approach allows different uncertainties to be obtained for each sub-basin for use in the integration process. For example, if certain water component estimates are less uncertain for an upstream basin, these estimates will have more weight for constraining the water balance downstream.

Figure 4 shows the long-term mean (top) of estimates throughout the Amazon basin. Precipitation is higher over the northern (6-Serrinha) and central (5-Manacapuru) regions of the basin, and evapotranspiration shows a similar pattern, with large transpiration from tropical forests. The variation of dS is greatest near the delta, where the amount of surface water associated with the river is the largest. For these three water components, discrepancies exist in the long-term mean between southern and northern sub-basins and the hydrological cycle appears to be more intense in the north (e.g., heavier rain, greater evapotranspiration, and larger changes in water storage). These local features can be observed only at the sub-basin scale with the northern and southern basins considered separately. If the entire basin had been considered instead, the average hydrological cycle would not have been representative of the southern region, where the water signal is relatively small.

Figure 4 shows the standard deviation (bottom) of these estimates. Over the entire Amazon at Obidos, the *a priori* uncertainty is 11.2 mm/month for P, 12.3 mm/month for E, 6.1 mm/month for dS, and 5.0 mm/month R. As shown in Figure 4, these uncertainties vary at the sub-basin scale. Uncertainty of P is elevated in 1-Tabatinga. This result might be related to the relative lack of gauge precipitation data from this mountainous region. Therefore, the estimates in that sub-basin have more degrees of freedom. E uncertainty broadly follows the mean values, with higher uncertainty in the northern and central areas. dS also has high uncertainty for the mountainous 1-Tabatinga sub-basin and the smallest sub-basin 7-Caracarai (due to the small scale of mountain glaciers and its impact on leakage error in GRACE product). On the contrary, the signal-to-noise ratio is higher over 2-Porto-Velho, while the ranges of variation are similar among these sites. For the *in situ* R, uncertainty was determined to be 7% of the long-term mean. This value is taken from Sahoo et al. (2011) and allows to describe spatial variation of the uncertainty with the magnitude of the discharge over the various sub-basins, from 5 mm/month in 1-Tabatinga to 30 mm/month in 10-Obidos. All the uncertainties estimated at the sub-basin scale are used to construct an *a priori* covariance matrix B_{SW} qualifying the *a priori* estimate. No cross-terms are included in B_{SW}; as a simplification, this means that no linking of errors occurs among sub-basins.

Translating the original *a priori* error estimates in *mm/month* into "uncertainty weight," in%, that describes the ratio between the uncertainty of a particular water component over the sum of all the uncertainty, may be useful. These weights are sometimes referred to as the "imbalance contribution" in the literature (Pan et al., 2012; Sahoo et al., 2011), as they drive the distribution of water budget residuals during integration. Table 4 provides uncertainty weights for Amazon WC obtained from the literature. As these uncertainty weight estimates are certain to vary with the method used and source of water component estimates, that information was also included in Table 4 for comparison. Besides the method and inputs, the uncertainty weight is also impacted by each other weight. For instance, the more uncertain is P estimate, the bigger is its uncertainty weight. This leads also to reduce the E weight. Even when the input data and method differ,

Table 4
Literature Comparison on the Uncertainty Weights (in%) Associated to the a priori Estimate for the Terrestrial Water Components Over the Amazon Basin

Studies		*P*	*E*	*dS*	*R*
Azarderakhsh et al. (2011)	Uncertainty weight	43	30	17	11
	Observation type	EO	EO	GRACE	*in situ*
	Method		Literature review		
Pan et al. (2012)	Uncertainty weight	38	25	25	12
	Observation type	*in situ*	EO, ERA, VIC	GRACE, VIC	*in situ*, VIC
	Method	Gauge density	dispersion of ensemble	10%-5% of value	10% of value
Sahoo et al. (2011)	Uncertainty weight	40	38	7	15
	Observation type	EO	EO	GRACE	*in situ*
	Method		dist. to non-satellite estimate	Rodell et al. (2004)	7% of the value
Zhang et al. (2018)	Uncertainty weight	45	22	24	9
	Observation type	EO	EO	GRACE, VIC	VIC
	Method		dispersion of ensemble	10%-5% of value	10% of value
Moreira et al. (2019b)	Uncertainty weight	45	22	24	9
	Observation type	EO	EO	GRACE	*in situ*
	Method		distance to *in situ* estimate	Rodell et al. (2004)	10% of the value
Our study	Uncertainty weight	32	36	18	14
	Observation type	EO, ERA	EO, ERA	GRACE*	*in situ*
	Method		dispersion of ensemble		7% of value

Note. Abbreviations: GRACE, Gravity Recovery and Climate Experiment; EO, Earth Observations; VIC, variable infiltration capacity.
[a]Only the current study uses the two kinds of solutions from GRACE (Spherical and MASCON) based on five products.

uncertainty weights broadly agree among studies focusing on the Amazon basin. The river discharge represents 15% of the total error while GRACE *dS* is 17% (resp. 25%) when used alone (resp. with model outputs. Finally, *P* and *E* share the bigger weights between 30% and 40% each.

The nature of the water component estimates and the method used to infer uncertainty weight vary among studies. Nevertheless, the uncertainty weights obtained here are broadly similar to those in the literature, with higher weights for *P* and *E*, followed by *dS* and finally *R*. Compared to other studies, the weights found here are more equally distributed among water components. Relatively greater weight was obtained here for *E* compared to *P*, which may be due to all precipitation estimates used in this study being calibrated with non-satellite data. The GRACE-derived uncertainty weight shows the largest variability among studies due to (1) the type of input used for *dS* (observation only or with model outputs) and (2) the different assumptions taken to estimate the *dS* uncertainty (see Table 4). The present study uses all global GRACE solutions including the spherical and MASCON-based solutions while estimating the *dS* uncertainty based on the spread of the datasets.

4.3. Post-Filtering (PF)-Based Integrated Solution

Once the *a priori* estimate X_{SW} of the WC is obtained along with the associated error covariance matrix B_{lo}, an integration approach is used to ensure the closure of the water budget (Aires et al., 2002; Pellet et al., 2019). The water balance closure of Equation 6 can be used to "update" X_{SW} to the integrated solution X_{PF}. This is done using a Bayesian estimator (Rodgers, 2000):

$$X_{PF} = (I - K_{PF} \cdot G_{am}\Sigma^{-1}G_{am}^{t}) \cdot X_{SW}, \tag{8}$$

where $K_{PF} = (B_{am}^{-1} + G_{am}\Sigma^{-1}G_{am}^{t})^{-1}$ and *PF* represents the "Post-Filtering" of the previous solution X_{SW}. With this methodology, the solution X_{PF} closes the water budget (within the relaxation term *r*) over the ten sub-basins considered.

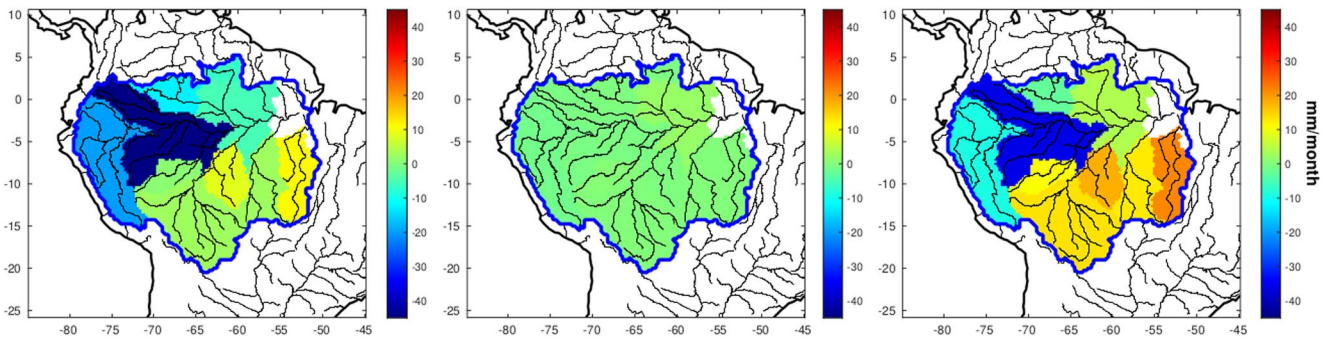

Figure 5. Annual mean water budget imbalance (in mm/month) over 10 sub-basins before integration (left), after SAWC integration accounting for interdependent sub-basins (middle), and after integration over the entire basin scale (right). For comparison purposes, the colorbar is defined based on the left figure, and the annual mean imbalance after SAWC (middle) varied by ± 2 mm/month. SAWC, Satellite water cycle.

4.4. Calibration of SAtellite Water Cycle (SAWC) Estimates

Integration introduces hydrological coherency at the sub-basin scale, constraining the spatial averages of all water fluxes. This estimate provides a reference, but it applies only to the ten sub-basins that were used for integration and the common period of all water component estimates.

To avoid these limitations, a calibration step based on statistical regression between the merged observations X_{SW} and the optimized estimates X_{PF} was used (Munier et al., 2014; Pellet et al., 2019, 2020). Because the merged observations X_{SW} are available at the pixel scale, calibration allows for spatialization of hydrological coherency at the sub-basin scale. The calibration is not strictly linear to avoid correcting null water fluxes (Pellet et al., 2019). The following regression was used for P, E, and dS:

$$Y_{SAWC} = a \cdot Y_{SW} + b \cdot \left(1 - e^{\frac{-Y_{SW}}{c}}\right) \tag{9}$$

where a, b, and c are calibration parameters that can vary from month to month. Because this regression method does not perfectly retrieve X_{PF} from X_{SW}, the calibration step does not close the WC balance (Munier & Aires, 2018; Pellet et al., 2019), but X_{SAWC} reduces water budget residuals for the entire sub-basin and has the original pixel-scale resolution of X_{SW}.

Figure 6 compares rows containing the original SW and SAWC values with CDR estimates for the four water components with water budget residuals in the 10-Manacapuru sub-basin throughout 2000–2015. E is strongly impacted by the integration and calibration processes due to the high uncertainty in E for this particular sub-basin. The resulting water budget residuals are much smaller for the calibrated solution, indicating that this solution is more coherent hydrologically.

Figure 5 illustrates an imbalance of the WC budget. To measure the benefit of sub-basin scale optimization, we compared integrations conducted at the basin and sub-basin scales. Total river discharge is the sum of the discharge for 10-Obidos, 9-Itaituba, and 8-Altamira, while the drainage area used to compute the spatially averaged estimates is the sum of the three drainage areas. Figure 5 (left) shows the annual mean imbalance over all Amazon sub-basins. The imbalance is greatest (25 mm/month) for the 5-Manacapuru sub-basin and smallest (7 mm/month) for sub-basin 10-Obidos. Analyzing the WC at the sub-basin scale allows various hydrological regimes to be considered separately. In Figure 5 (left), a gradient exists between the northern and southern sub-basins. Northern sub-basins show a lack of water (e.g., negative long-term mean imbalance), while southern sub-basins show an excess of water. This pattern exists only at the sub-basin scale, and thus considering the basin as a whole would lead to loss of information on these two regimes in averaged values. When calculated as a basin average, the hydrological signal is driven by the northern sub-basins, and the average WC budget imbalance is negative over the entire basin (not shown). Integration at the entire basin scale can be used to identify the best compromise, but the resulting correction will not reflect the diversity of sub-basins present. As a result, the average residual value over the entire basin does not exceed 2 mm/month (not shown), but strong sub-basin imbalances remain, as shown in Figure 5 (middle).

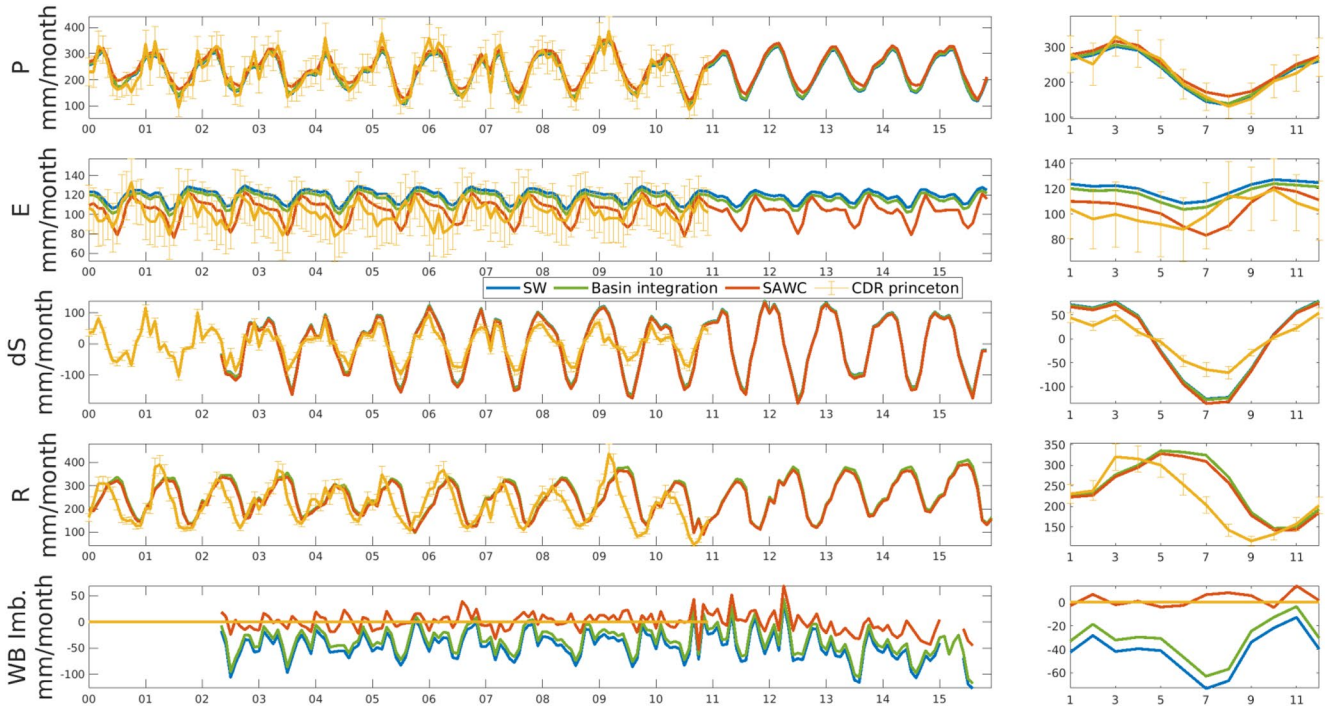

Figure 6. WC components over the 5-Manacapuru drainage area: Simple Weigthing (blue), Basin-scale integration (green), SAWC (red), CDR (orange) from (Zhang et al., 2018). Error-bar shows the uncertainty estimated in the CDR dataset. Right column shows the climatological season computed over 2002–2015 for all the estimates. SAWC, Satellite water cycle.

Optimizing the estimation of water components based on the water conservation over the entire basin is a good compromise in general, but this approach cannot handle regional specificity. Figure 5 (right) shows how the water budget residuals are impacted by SAWC; the water balance is improved over all 10 sub-basins of the Amazon and does not exceed 2 mm/month for any sub-basin. The SAWC approach allows handling of regional WC monitoring to preserve spatial coherency among all sub-basins. Optimizing the sub-basins independently would allow the imbalance to be reduced, but the spatial dependency would be lost. For example, river discharge would be optimized independently for upstream and downstream sub-basins.

4.5. SAWC Evaluation

The WC analysis method used here is called the SAWC database. In Figure 6, the SW (blue), basin-scale integration (green), SAWC (red), and CDR (yellow) water budgets are compared. The first four rows indicate how the SAWC water balance impacts each water component, while the last row shows the budget residuals. Compared to SW, SAWC better closed the WC, with relatively small changes in the estimates of water components. The E estimate changed most in this sub-basin with the SAWC approach. This change may be related to the uncertainties shown in Figure 4 (bottom). Compared to basin-scale integration, the SAWC approach allows for better optimization of water components. While basin-scale integration primarily impacted the two main fluxes, P, and E, SAWC also optimized the estimates of river discharge R at the sub-basin scale. Basin-scale optimization was based on the estimates averaged over the entire basin, and large-scale balance can be obtained without ensuring local balance in all sub-basins. In contrast, SAWC supports hydrological coherency at the regional scale.

When compared, E is similar to CDR estimates. The CDR data set closes the water budget at the VIC pixel (with a residual value of zero in the fifth row) when the VIC runoff and VIC + GRACE merged estimate for dS are used, which explains the large differences in R (fourth row). In a previous study (Zhang et al., 2018), the unofficial R value was the amount of water that is not routed but departs from the continental surface over a month. This variable cannot be compared to R straightforwardly estimated from river discharge. The differences in dS are caused by VIC simplifying the physical process at the origin of dS, in particular by

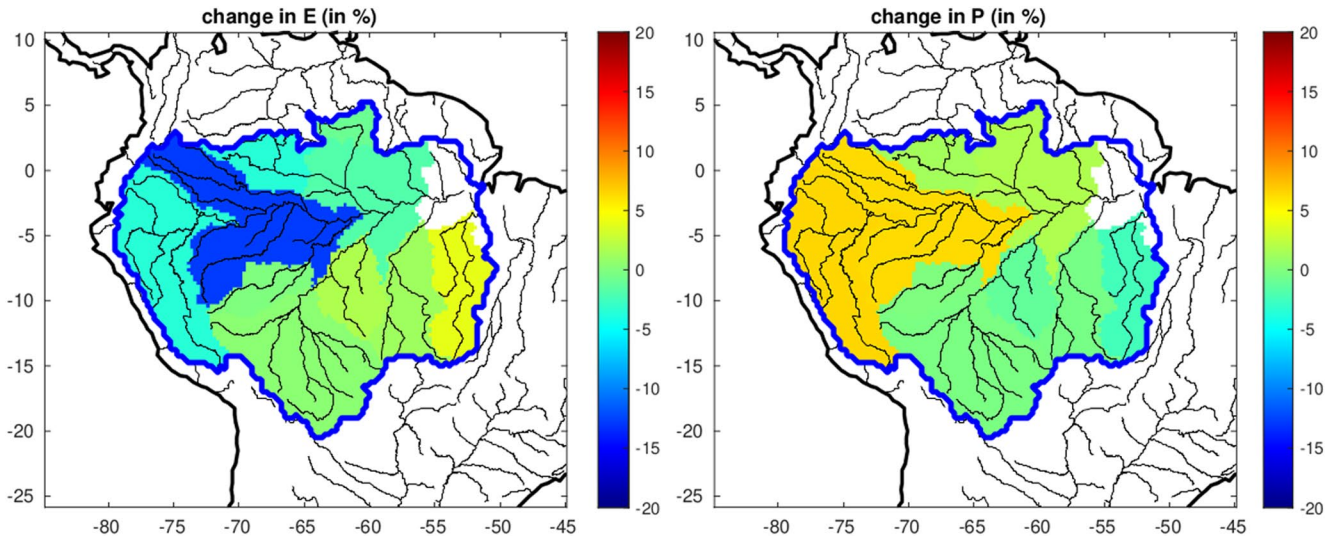

Figure 7. Change (in %) in the long term *E* (left) and *P* (right) means with the SAWC approach. SAWC, Satellite water cycle.

excluding groundwater from consideration. Finally, estimates of the two vertical fluxes, *P*, and *E*, appear coherent. This result highlights the inclusion of information about horizontal water movement in the GRACE observations, as this information is not used in the VIC model. If the calibration process does not perfectly close the WC, the residuals are strongly reduced by using SAWC.

While SAWC allows for strongly reducing the WC budget residuals (last row of Figure 6), the procedure might make the various water component estimates get away from their *a priori* estimates. Figure 7 represents the impact of SAWC on the two main fluxes, *P* and *E*. In other words, how far the WC closure has modified these fluxes from their *a priori* estimates. For *E*, this impact ranges from −7% in 5-Manacapuru to 5% in 10-Obidos. *P* is impacted most strongly in 1-Tabatinga (5%) and Altamira (−5%). This figure shows that hydrological coherence can be attained even with relatively small changes in the estimates. If the impacts are low, they still differ at the sub-basin scale. The 5-Manacapuru sub-basin shows the highest change in the two fluxes raising concern about estimated *P* and *E* from a satellite over the dense tropical forest.

Table 5 provides a comparison of the HYBAM-observed precipitation (HOP) gridded gauge precipitation data set (Section 3) with those resulting from SAWC, the integration approach considering only closure at the Amazon outlet, CDR, and input (MSWEP, TMPA, ERA5) estimates for each sub-basin based on temporal correlation (at the monthly and sub-basin scales), along with root-mean-square deviation (RMSD) values. For all sub-basins, the SAWC methodology performs as well as or better than other statistical estimates. Although the correlation between the input estimate and HOP was already good, SAWC improved the correlation to 0.96 for sub-basin 5-Manacapuru. This improvement was observed even over complex mountainous sub-basins, such as 1-Tabatinga (0.97). SAWC also reduced the RMSD for HOP compared to the input data.

Compared with CDR estimates, SAWC consistently performs better, except over sub-basin 5-Manacapuru. These results illustrate the positive effect of the closure constraint on precipitation when using observation for *dS* and *R*. While the CDR approach is limited by the use of VIC output for runoff and *dS* (in particular horizontal routing of the runoff is not considered in *R* nor VIC *dS*), SAWC can better take into account this exchange and this results in a better correction of P. Even without explicitly constraining the satellite precipitation products to align with *in situ* data, the SAWC statistics shows improved performance. SAWC is slightly better than the one-basin method, both in terms of correlation and RMSD. In 1-Tabatinga, the precipitation pattern is driven by the forcing from the mountains, while precipitation is primarily driven by the monsoon. SAWC can better use these local features than other methods.

Figure 8 depicts the climatology (2002–2015, in mm/month) of the water budget over the Amazon before (dashed line) and after (continuous line) the SAWC optimization. This description highlights spatial

10.1029/2020WR028647

Table 5
Comparison of the P Estimates With the SO-HYBAM Gauge Measurements

	CORRELATION						RMSD (in mm/month)					
Basin	CDR	Integration at the outlet	SAWC	ERA5	TMPA	MSWEP	CDR	Integration at the outlet	SAWC	ERA5	TMPA	MSWEP
1-Tabatina	0.78	0.96	0.97	0.94	0.94	0.94	41	33	34	27	32	29
2-Porto-velho	0.98	0.99	0.99	0.98	0.99	0.98	19	20	16	20	17	20
3-Labrea	0.95	0.98	0.99	0.97	0.96	0.98	33	19	18	24	29	19
4-Fz-vista	0.96	0.98	0.98	0.97	0.97	0.99	37	24	25	32	32	24
5-Manacapuru	0.94	0.95	0.96	0.94	0.93	0.94	26	22	20	24	28	26
6-Serrinha	0.84	0.93	0.94	0.91	0.87	0.93	45	28	27	32	39	28
7-Caracarai	0.94	0.96	0.96	0.94	0.95	0.95	73	42	41	44	45	40
8-Altamira	0.97	0.98	0.98	0.97	0.97	0.98	35	25	24	27	31	23
9-Itaituba	0.97	0.99	0.99	0.98	0.98	0.99	35	22	20	26	28	19
10-Obidos	0.89	0.98	0.97	0.96	0.95	0.98	41	29	29	32	33	25

Abbreviations: CDR, climate data record; RMSD, root mean square density; MSWEP, Multisource Weighted Ensemble Participation; SAWC, Satellite water cycle; TMPA, Tropical Rainfall Measuring Mission Multisatellite Precipitation Analysis.

patterns of the Amazon water cycle with differences between the northern and southern basins (Espinoza et al., 2019; Marengo, 2005). Over the southern basin, *P* is driven by the monsoon with a peak in January and shows a larger seasonal variation (e.g., min-max range) and lower annual mean than on over the northern basins, where the P peak is reached in May. *P* drives *R* season over the upstream sub-basins with a time lag of 1–2 months between *P* and *R*. Over northern and central sub-basins, *dS* becomes negative while R is still increasing (and reaches its maximum 2 months later). This illustrates the floodplain buffer effect that charged water before releasing it into the river (Sorribas et al., 2020). *E* seasonal variation is weaker than for *P* but *E* peak seems to be in phase with P over southern basin arguing for a water-limited behavior (Espinoza

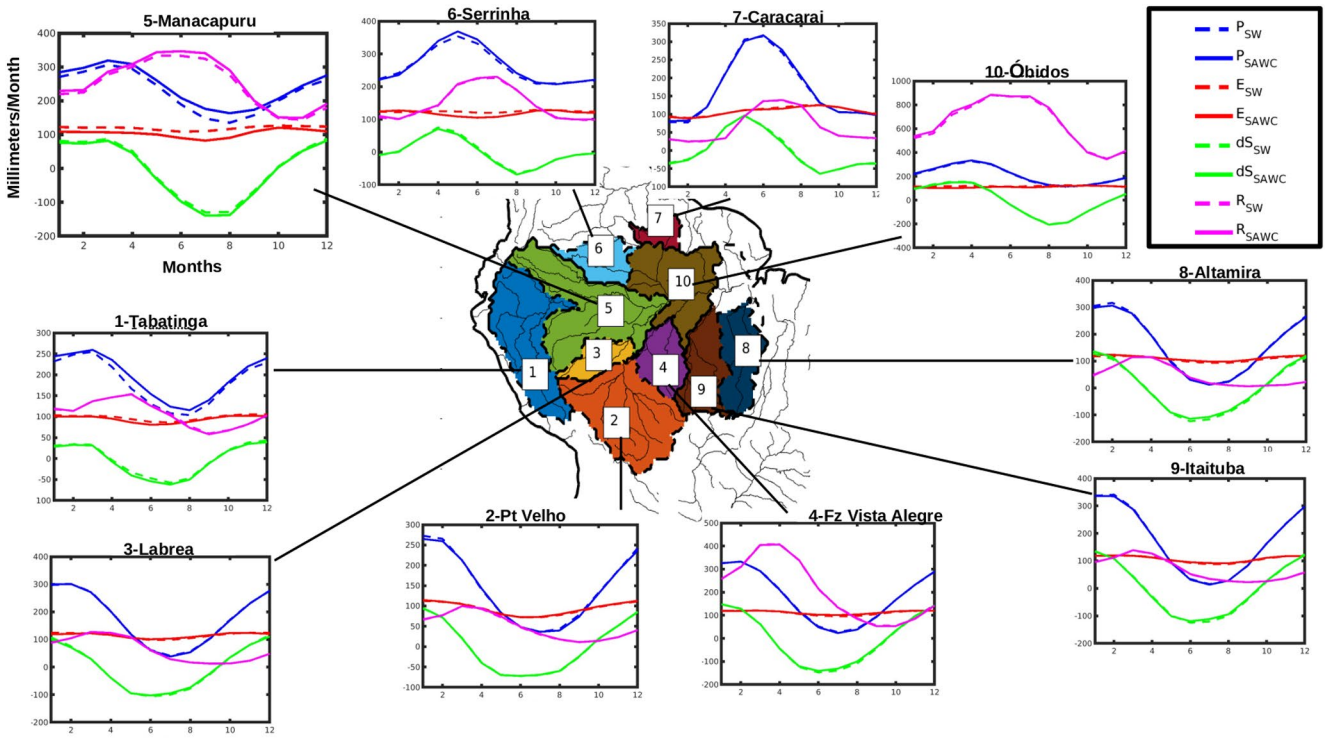

Figure 8. Climatology (2002–2015) of the water budget over the Amazon before (dashed line) and after (continuous line) optimization.

et al., 2019; Sörensson & Ruscica, 2018) while E peak follows P minimum month in northern basin depicting energy-limited system (Espinoza et al., 2019). In the South, during dry months (JJA), E is higher than P, and water that evaporates is provided by the soil storage which continues to lose water until November. For this season, the role of E on the water cycle is relatively more important in the dry season than in the rainy season (Marengo, 2005). The correction implied by SAWC varies over sub-basins. The 5-Manacapuru shows the biggest correction with 1-Tabatinga and 6-Serrinha. Overall, The SAWC optimization increased E seasonal variation and the P annual mean.

5. Conclusion and Perspectives

In this paper, the SAWC methodology is presented. It allows hydrologically coherent monitoring of the water cycle at sub-basin scale over the Amazon basin. Compared to previous optimization frameworks based on the water budget closure, spatial information is introduced into the SAWC optimization scheme by adding constraints on horizontal water exchanges among sub-basins that are inter-dependently closed. These constraints help improve the water component estimates. SAWC allows the average WC budget residuals to be reduced to 2 mm/month over all sub-basins. The datasets from SAWC analysis are freely available at https://data.mendeley.com/datasets/4bybp4r355/draft?a=b59dbab2-37c0-4305-b3cd-05775566371c (will be published with the paper).

SAWC allows for the correction of satellite databases at the sub-basin scale, which is better suited to the variety of hydrological regimes present in the Amazon basin (Builes-Jaramillo & Poveda, 2018; Marengo, 2005). The methodology avoids mixing the rain peak signals from southern and northern regions with those from mountainous regions (the Andes) that do not exhibit a monsoon precipitation pattern. Evaluated with *in situ* data, satellite-based precipitation data set is improved, when the WC is balanced, compared with the original estimates. SAWC correction suggests a positive bias in precipitation over Andes mountainous and central areas.

Evapotranspiration estimated based on satellite data shows the highest uncertainty among water components. Dispersion among datasets is large, and incoherence among WC components can be large in some sub-basins. Estimation of evaporation in tropical areas covered with dense vegetation is known to be a challenge. As a consequence, the integration scheme for satellite observations includes major corrections for evaporation in some sub-basins. There is a lot of effort in the literature trying to better understand the limitation of E based on energy and water supplies (Builes-Jaramillo & Poveda, 2018; Maeda et al., 2017; Swann & Koven, 2017). The SAWC indicates the water (resp. energy) limitation in E season over central (resp. northern) sub-basins. Unfortunately, it is very difficult to validate these corrections using *in situ* measurements. New ways of evaluating and calibrating evaporation datasets must be developed to improve our understanding of the WC.

We compared our purely observational SAWC analysis to CDR estimation of water components. The differences between their results show the advantage of using the GRACE measurements in contrast to most assimilation databases. Land surface models generally do not assimilate GRACE measurements. This is an ongoing research (Girotto et al., 2019; Li et al., 2019). Model simulations can be used to estimate synthetic dS for comparison, but assimilating these differences into the model by changing different state variables is challenging. Thus, GRACE measurements are generally used in this context only as an *a posteriori* evaluation. Failing to use GRACE data is a major drawback, as dS provides very important information about the overall WC.

The SAWC methodology provides the most coherent description of the WC at the sub-basin scale. This unprecedented observation-based dataset will be used further. In companion paper 2, the present SAWC analysis tool is used to estimate missing water components, including an extension of dS back in time, before the GRACE era. SAWC is also used to spatially estimate river discharge measurements from various stations along the river.

Data Availability Statement

All original datasets used in the study are described in Table 3 and can be freely accessed from the data producer. The dataset from SAWC analysis is freely available at https://data.mendeley.com/datasets/4bybp4r355/draft?a=b59dbab2-37c0-4305-b3cd-05775566371c (will be published with the paper).

Acknowledgments
The study has been supported by the JSPS Kakenhi (N16H06291). Victor Pellet was founded by JSPS Postdoctoral Fellowships for Research in Japan. The author would like to thank Ayan santos fleischmann for providing the ANA river discharge measurements. The author wants to thank the two anonymous reviewers that help to improve the manuscript.

References

Abolafia-Rosenzweig, R., Pan, M., Zeng, J. L., & Livneh, B. (2021). Remotely sensed ensembles of the terrestrial water budget over major global river basins: An assessment of three closure techniques. *Remote Sensing of Environment*, *252*, 112191. https://doi.org/10.1016/j.rse.2020.112191

Aires, F. (2014). Combining datasets of satellite-retrieved products. Part I: Methodology and water budget closure. *Journal of Hydrometeorology*, *15*(4), 1677–1691. https://doi.org/10.1175/JHM-D-13-0148.1

Aires, F., Rossow, W. B., Scott, N. A., & Chédin, A. (2002). Remote sensing from the infrared atmospheric sounding interferometer instrument 1. Compression, denoising, and first-guess retrieval algorithms. *Journal of Geophysical Research - D: Atmospheres*, *107*(D22), 3517. https://doi.org/10.1029/2001JD000955

Alsdorf, D. E., Smith, L. C., & Melack, J. M. (2001). Amazon floodplain water level changes measured with interferometric SIR-C radar. *IEEE Transactions of Geosciences and Remote Sensing*, *39*(2), 423–431. https://doi.org/10.1109/36.905250

Azarderakhsh, M., Rossow, W. B., Papa, F., Norouzi, M., & Khanbilvardi, R. (2011). Diagnosing water variations with the Amazon basin using satellite data. *Journal of Geophysical Research*, *116*, D24107. https://doi.org/10.1029/2011jd015997

Barlow, J., Lennox, G. D., Ferreira, J., Berenguer, E., Lees, A. C., Nally, R. M., et al. (2016). Anthropogenic disturbance in tropical forests can double biodiversity loss from deforestation. *Nature*, *535*(7610), 144–147. https://doi.org/10.1038/nature18326

Beck, H. E., van Dijk, A. I. J. M., Levizzani, V., Schellekens, J., Miralles, D. G., Martens, B., & de Roo, A. (2017). MSWEP: 3-hourly 0.25° global gridded precipitation (1979-2015) by merging gauge, satellite, and reanalysis data. *Hydrology and Earth System Sciences*, *21*(1), 589–615. https://doi.org/10.5194/hess-21-589-2017

Beck, H. E., Wood, E. F., Pan, M., Fisher, C. K., Miralles, D. G., Van Dijk, A. I. J. M., et al. (2019). MSWEP V2 Global 3-Hourly 0.1° precipitation: Methodology and quantitative assessment. *Bulletin of the American Meteorological Society*, *100*(3), 473–500. https://doi.org/10.1175/BAMS-D-17-0138.1

Bettadpur, S. (2012). *GRACE 327-742 (CSR-GR-12-xx) gravity RECOVERY and climate experiment UTCSR Level-2 processing standards Document) (for Level-2 product Release 0005)*.

Biancamaria, S., Lettenmaier, D. P., & Pavelsky, T. M. (2016). *The SWOT mission and its Capabilities for land hydrology*. In (pp. 117–147). Springer, Cham. https://doi.org/10.1007/978-3-319-32449-4_6

Builes-Jaramillo, A., & Poveda, G. (2018). Conjoint analysis of surface and atmospheric water balances in the Andes-Amazon system. *Water Resources and Research*, *54*(5), 3472–3489. https://doi.org/10.1029/2017WR021338

Callède, J., Cochonneau, G., Alves, F. V., Guyot, J.-L., Guimarães, V. S., De Oliveira, E., & De Oliveira, E. (2010). Les apports en eau de l'Amazone à l'Océan Atlantique. *rseau*, *23*(3), 247–273. https://doi.org/10.7202/044688ar

Callede, J., Kosuth, P., & De Oliveira, E. (2001). Etablissement de la relation hauteur-débit de l'Amazone à Óbidos: Méthode de la dénivelée normale à "géométrie variable". *Hydrological Sciences Journal*, *46*(3), 451–463. https://doi.org/10.1080/02626660109492838

Chaudhari, S., Pokhrel, Y., Moran, E., & Miguez-Macho, G. (2019). Multi-decadal hydrologic change and variability in the Amazon River basin: Understanding terrestrial water storage variations and drought characteristics. *Hydrology and Earth System Sciences*, *23*(7), 2841–2862. https://doi.org/10.5194/hess-23-2841-2019

Dahle, C., Flechtner, F., Gruber, C., König, D., König, R., Michalak, G., & Neumayer, K.-H. (2013). *GFZ GRACE Level-2 processing standards Document for Level-2 product Release 0005*.

Dee, D. P., Uppala, S. M., Simmons, A. J., Berrisford, P., Poli, P., Kobayashi, S., et al. (2011). The ERA-Interim reanalysis: Configuration and performance of the data assimilation system. *Quarterly Journal of the Royal Meteorological Society*, *137*(656), 553–597. https://doi.org/10.1002/qj.828

Durand, M., Fu, L.-L., Lettenmaier, D. P., Alsdorf, D. E., Rodriguez, E., & Esteban-Fernandez, D. (2010). The surface water and ocean topography mission: Observing terrestrial surface water and oceanic submesoscale eddies. *Proceedings of the IEEE*, *98*(5), 766–779. https://doi.org/10.1109/JPROC.2010.2043031

Espinoza, J. C., Ronchail, J., Guyot, J. L., Junquas, C., Vauchel, P., Lavado, W., et al. (2011). Climate variability and extreme drought in the upper Solimões River (western Amazon Basin): Understanding the exceptional 2010 drought. *Geophysical Research Letters*, *38*(13). https://doi.org/10.1029/2011GL047862

Espinoza, J. C., Sörensson, A. A., Ronchail, J., Molina-Carpio, J., Segura, H., Gutierrez-Cori, O., et al. (2019). Regional hydro-climatic changes in the Southern Amazon Basin (Upper Madeira Basin) during the 1982-2017 period. *Journal of Hydrology: Regional Studies*, *26*, 100637. https://doi.org/10.1016/j.ejrh.2019.100637

Espinoza Villar, J. C., Ronchail, J., Guyot, J. L., Cochonneau, G., Naziano, F., Lavado, W., et al. (2009). Spatio-temporal rainfall variability in the Amazon basin countries (Brazil, Peru, Bolivia, Colombia, and Ecuador). *International Journal of Climatology*, *29*(11), 1574–1594. https://doi.org/10.1002/joc.1791

Girotto, M., Reichle, R. H., Rodell, M., Liu, Q., Mahanama, S., & De Lannoy, G. J. M. (2019). Multi-sensor assimilation of SMOS brightness temperature and GRACE terrestrial water storage observations for soil moisture and shallow groundwater estimation. *Remote Sensing of Environment*, *227*, 12–27. https://doi.org/10.1016/j.rse.2019.04.001

Guimberteau, M., Ciais, P., Ducharne, A., Boisier, J. P., Dutra Aguiar, A. P., Biemans, H., et al. (2017). Impacts of future deforestation and climate change on the hydrology of the Amazon Basin: A multi-model analysis with a new set of land-cover change scenarios. *Hydrology and Earth System Sciences*, *21*(3), 1455–1475. https://doi.org/10.5194/hess-21-1455-2017

Guimberteau, M., Drapeau, G., Ronchail, J., Sultan, B., Polcher, J., Martinez, J.-M., et al. (2012). Discharge simulation in the sub-basins of the Amazon using ORCHIDEE forced by new datasets. *Hydrology and Earth System Sciences*, *16*(3), 911–935. https://doi.org/10.5194/hess-16-911-2012

Guimberteau, M., Ronchail, J., Espinoza, J. C., Lengaigne, M., Sultan, B., Polcher, J., et al. (2013). Future changes in precipitation and impacts on extreme streamflow over Amazonian sub-basins. *Environmental Research Letters*, *8*(1), 014035. https://doi.org/10.1088/1748-9326/8/1/014035

Hersbach, H., Bell, B., Berrisford, P., Hirahara, S., Horányi, A., Muñoz-Sabater, J., et al. (2020). The ERA5 global reanalysis. *Quarterly Journal of the Royal Meteorological Society*, *146*(730), 1999–2049. https://doi.org/10.1002/qj.3803

Huffman, G. J., Bolvin, D. T., Nelkin, E. J., Wolff, D. B., Adler, R. F., Gu, G., et al. (2007). The TRMM multisatellite precipitation analysis (TMPA): Quasi-global, multiyear, combined-sensor precipitation estimates at fine scales. *Journal of Hydrometeorology*, *8*(1), 38–55. https://doi.org/10.1175/JHM560.1

Kim, H., Yeh, P. J.-F., Oki, T., & Kanae, S. (2009). Role of rivers in the seasonal variations of terrestrial water storage over global basins. *Geophysical Research Letters*, *36*(17), L17402. https://doi.org/10.1029/2009GL039006

Landerer, F. W., Dickey, J. O., & Güntner, A. (2010). Terrestrial water budget of the Eurasian pan-Arctic from GRACE satellite measurements during 2003-2009. *Journal of Geophysical Research*, *115*(23), 1–14. https://doi.org/10.1029/2010JD014584

Latrubesse, E. M., Arima, E. Y., Dunne, T., Park, E., Baker, V. R., d'Horta, F. M., et al. (2017). Damming the Rivers of the Amazon Basin. (Vol. 546, pp. 363–369). Nature Publishing Group. https://doi.org/10.1038/nature22333

Li, B., Rodell, M., Kumar, S., Beaudoing, H. K., Getirana, A., Zaitchik, B. F., et al. (2019). Global GRACE data assimilation for groundwater and drought monitoring: Advances and challenges. *Water Resources and Research*, *55*(9), 7564–7586. https://doi.org/10.1029/2018WR024618

Liu, J., Shangguan, D., Liu, S., Ding, Y., Wang, S., & Wang, X. (2019). Evaluation and comparison of CHIRPS and MSWEP daily-precipitation products in the Qinghai-Tibet Plateau during the period of 1981-2015. *Atmospheric Research*, *230*, 104634. https://doi.org/10.1016/j.atmosres.2019.104634

Maeda, E. E., Ma, X., Wagner, F. H., Kim, H., Oki, T., Eamus, D., & Huete, A. (2017). Evapotranspiration seasonality across the Amazon Basin. *Earth Systems and Dynamics*, *8*(2), 439–454. https://doi.org/10.5194/esd-8-439-2017

Marengo, J. A. (2005). Characteristics and spatio-temporal variability of the Amazon river basin water budget. *Climate Dynamics*, *24*(1), 11–22. https://doi.org/10.1007/s00382-004-0461-6

Marengo, J. A., Souza, C. M., Thonicke, K., Burton, C., Halladay, K., Betts, R. A., et al. (2018). Changes in climate and land use over the Amazon region: Current and future variability and trends. *Frontiers of Earth Science*, *6*, 228. https://doi.org/10.3389/feart.2018.00228

Marengo, J. A., Tomasella, J., Alves, L. M., Soares, W. R., & Rodriguez, D. A. (2011). The drought of 2010 in the context of historical droughts in the Amazon region. *Geophysical Research Letters*, *38*(12). https://doi.org/10.1029/2011GL047436

Martens, B., Miralles, D. G., Lievens, H., van der Schalie, R., de Jeu, R. A. M., Férnandez-Prieto, D., et al. (2017). GLEAM v3: satellite-based land evaporation and root-zone soil moisture. *Geoscientific Model Development Discussions*, *10*, 1903–1925. https://doi.org/10.5194/gmd-10-1903-2017

Michel, D., Jiménez, C., Miralles, D. G., Jung, M., Hirschi, M., Ershadi, A., et al. (2016). The WACMOS-ET project - Part 1: Tower-scale evaluation of four remote-sensing-based evapotranspiration algorithms. *Hydrology and Earth System Sciences*, *20*(2), 803–822. https://doi.org/10.5194/hess-20-803-2016

Miralles, D. G., De Jeu, R. A. M., Gash, J. H., Holmes, T. R. H., & Dolman, A. J. (2011). Magnitude and variability of land evaporation and its components at the global scale. *Hydrology and Earth System Sciences*, *15*, 967–981.Retrieved from www.hydrol-earth-syst-sci.net/15/967/2011/

Monteith, J. L. (1965). Evaporation and Environment (Vol. 19).

Moreira, A. A., Ruhoff, A. L., Roberti, D. R., Souza, V. d. A., da Rocha, H. R., & Paiva, R. C. D. d. (2019a). Assessment of terrestrial water balance using remote sensing data in South America. *Journal of Hydrology*, *575*(May), 131–147. https://doi.org/10.1016/j.jhydrol.2019.05.021

Moreira, A. A., Ruhoff, A. L., Roberti, D. R., Souza, V. d. A., da Rocha, H. R., & Paiva, R. C. D. d. (2019b). Assessment of terrestrial water balance using remote sensing data in South America. *Journal of Hydrology*, *575*, 131–147. https://doi.org/10.1016/j.jhydrol.2019.05.021

Moura, R. L., Amado-Filho, G. M., Moraes, F. C., Brasileiro, P. S., Salomon, P. S., Mahiques, M. M., et al. (2016). An extensive reef system at the Amazon River mouth. *Science Advances*, *2*(4), e1501252. https://doi.org/10.1126/sciadv.1501252

Munier, S., & Aires, F. (2018). A new global method of satellite dataset merging and quality characterization constrained by the terrestrial water budget. *Remote Sensing of Environment*, *205*(October 2017), 119–130. https://doi.org/10.1016/j.rse.2017.11.008

Munier, S., Aires, F., Schlaffer, S., Prigent, C., Papa, F., Maisongrande, P., & Pan, M. (2014). Combining data sets of satellite-retrieved products for basin-scale water balance study: 2. Evaluation on the Mississippi Basin and closure correction model. *Journal of Geophysical Research - D: Atmospheres*, *119*(21), 12100–12112. https://doi.org/10.1002/2014JD021953

Mu, Q., Zhao, M., & Running, S. W. (2011). Improvements to a MODIS global terrestrial evapotranspiration algorithm. *Remote Sensing of Environment*, *115*(8), 1781–1800.Retrieved from http://linkinghub.elsevier.com/retrieve/pii/S0034425711000691. https://doi.org/10.1016/j.rse.2011.02.019

Nobre, C. A., Sampaio, G., Borma, L. S., Castilla-Rubio, J. C., Silva, J. S., & Cardoso, M. (2016). Land-use and climate change risks in the amazon and the need of a novel sustainable development paradigm. *Proceedings of the National Academy of Sciences of the United States of America*, *113*(39), 10759–10768. https://doi.org/10.1073/pnas.1605516113

Oliveira, P. T. S., Nearing, M. A., Moran, M. S., Goodrich, D. C., Wendland, E., & Gupta, H. V. (2014 sep). Trends in water balance components across the Brazilian Cerrado. *Water Resources and Research*, *50*(9), 7100–7114. https://doi.org/10.1002/2013WR015202

Paiva, R. C. D., Collischonn, W., & Buarque, D. C. (2013). Validation of a full hydrodynamic model for large-scale hydrologic modelling in the Amazon. *Hydrological Processes*, *27*(3), 333–346. https://doi.org/10.1002/hyp.8425

Pan, M., Sahoo, A. K., Troy, T. J., Vinukollu, R. K., Sheffield, J., & Wood, E. F. (2012). Multisource estimation of long-term terrestrial water budget for major global river basins. *Journal of Climate*, *25*(9), 3191–3206. https://doi.org/10.1175/JCLI-D-11-00300.1

Pan, M., & Wood, E. F. (2006). Data assimilation for estimating the terrestrial water budget using a constrained ensemble Kalman Filter. *Journal of Hydrometeorology*, *7*(3), 534–547. https://doi.org/10.1175/JHM495.1

Pellet, V., Aires, F., Munier, S., Fernández Prieto, D., Jordá, G., Dorigo, W. A., et al. (2019). Integrating multiple satellite observations into a coherent dataset to monitor the full water cycle - Application to the Mediterranean region. *Hydrology and Earth System Sciences*, *23*(1), 465–491. https://doi.org/10.5194/hess-23-465-2019

Pellet, V., Aires, F., Papa, F., Munier, S., & Decharme, B. (2020). Long-term total water storage change from a Satellite Water Cycle reconstruction over large southern Asian basins. *Hydrology and Earth System Sciences*, *24*(6), 3033–3055.Retrieved from https://hess.copernicus.org/articles/24/3033/2020/. https://doi.org/10.5194/hess-24-3033-2020

Penman, H. L. (1948). Natural evaporation from open water, hare soil and grass. *Proceedings of the Royal Society of London A: Mathematics, Physics, Sci.*, *193*(1032), 120–145. https://doi.org/10.1098/rspa.1948.0037

Priestley, C. H. B., & Taylor, R. J. (1972). On the assessment of surface heat flux and evaporation using large-scale parameters. *Monthly Weather Review*, *100*(2), 81–92. https://doi.org/10.1175/1520-0493(1972)100⟨0081:otaosh⟩2.3.co;2

Rodell, M., Houser, P. R., Jambor, U., Gottschalck, J., Mitchell, K., Meng, C.-J., et al. (2004). The global land data assimilation system. *Bulletin of theAmerican Meteorological Society*, *85*(3), 381–394.Retrieved from https://journals.ametsoc.org/doi/pdf/10.1175/BAMS-85-3-381

Rodell, M., Mcwilliams, E. B., Famiglietti, J. S., Beaudoing, H. K., & Nigro, J. (2011). Estimating evapotranspiration using an observation based terrestrial water budget. *Hydrological Processes*, *25*(26), 4082–4092. https://doi.org/10.1002/hyp.8369

Rodgers, C. D. (2000). *Columbia University Authentication*. https://doi.org/10.1002/9781118165690

Sahoo, A. K., Pan, M., Troy, T. J., Vinukollu, R. K., Sheffield, J., & Wood, E. F. (2011). Reconciling the global terrestrial water budget using satellite remote sensing. *Remote Sensing of Environment*, *115*(8), 1850–1865. https://doi.org/10.1016/j.rse.2011.03.009

Sakumura, C., Bettadpur, S., & Bruinsma, S. (2014 mar). Ensemble prediction and intercomparison analysis of GRACE time-variable gravity field models. *Geophysical Research Letters*, *41*(5), 1389–1397. https://doi.org/10.1002/2013GL058632

Save, H., Bettadpur, S., & Tapley, B. D. (2016). High-resolution CSR GRACE RL05 mascons. *Journal of Geophysical Research: Solid Earth*, *121*(10), 7547–7569. https://doi.org/10.1002/2016JB013007

Scanlon, B. R., Zhang, Z., Save, H., Wiese, D. N., Landerer, F. W., Long, D., et al. (2016). Global evaluation of new GRACE mascon products for hydrologic applications. *Water Resources Research*, *52*(12), 9412–9429. https://doi.org/10.1002/2016WR019494

Schneider, U., Becker, A., Finger, P., Meyer-Christoffer, A., Ziese, M., Rudolf, B., & Schneider, U. (2011). GPCC's new land surface precipitation climatology based on quality-controlled in situ data and its role in quantifying the global water cycle. *Theoretical and Applied Climatology*, *115*(1–2), 15–40. https://doi.org/10.1007/s00704-013-0860-x

Schneider, U., Becker, A., Ziese, M., & Rudolf, B. (2014). *Global precipitation analysis products of the GPCC*. Internet Publ.(May), 1–13. Retrieved from ftp://ftp-anon.dwd.de/pub/data/gpcc/PDF/GPCC_intro_products_2008.pdf

Sheffield, J., Ferguson, C. R., Troy, T. J., Wood, E. F., & McCabe, M. F. (2009). Closing the terrestrial water budget from satellite remote sensing. *Geophysical Research Letters*, *36*(7). https://doi.org/10.1029/2009GL037338

Sörensson, A. A., & Ruscica, R. C. (2018). Intercomparison and uncertainty assessment of nine evapotranspiration estimates over South America. *Water Resources Research*, *54*(4), 2891–2908. https://doi.org/10.1002/2017WR021682

Sorribas, M. V., de Paiva, R. C. D., Fleischmann, A. S., & Collischonn, W. (2020). Hydrological tracking model for Amazon surface waters. *Water Resources Research*, *56*(9). https://doi.org/10.1029/2019WR024721

Su, F., Hong, Y., & Lettenmaier, D. P. (2008). Evaluation of TRMM multisatellite precipitation analysis (TMPA) and its utility in hydrologic prediction in the La Plata Basin. *Journal of Hydrometeorology*, *9*(4), 622–640.Retrieved from https://journals.ametsoc.org/view/journals/hydr/9/4/2007jhm944_1.xml. https://doi.org/10.1175/2007JHM944.1

Sun, Q., Miao, C., Duan, Q., Ashouri, H., Sorooshian, S., & Hsu, K. L. (2018). A review of global precipitation data sets: Data sources, estimation, and intercomparisons. *Reviews of Geophysics*, *56*(1), 79–107. https://doi.org/10.1002/2017RG000574

Swann, A. L. S., & Koven, C. D. (2017). A direct estimate of the seasonal cycle of evapotranspiration over the Amazon Basin. *Journal of Hydrometeorology*, *18*(8), 2173–2185.Retrieved from https://journals.ametsoc.org/view/journals/hydr/18/8/jhm-d-17-0004_1.xml. https://doi.org/10.1175/JHM-D-17-0004.1

Syed, T. H., Famiglietti, J. S., Chen, J., Rodell, M., Seneviratne, S. I., Viterbo, P., & Wilson, C. R. (2005). Total basin discharge for the Amazon and Mississippi River basins from GRACE and a land-atmosphere water balance. *Geophysical Research Letters*, *32*(24), L24404. https://doi.org/10.1029/2005GL024851

Tapley, B. D., Bettadpur, S., Watkins, M., & Reigber, C. (2004). The gravity recovery and climate experiment: Mission overview and early results. *Geophysical Research Letters*, *31*. https://doi.org/10.1029/2004GL019920

Ward, N. D., Krusche, A. V., Sawakuchi, H. O., Brito, D. C., Cunha, A. C., Moura, J. M. S., et al. (2015). The compositional evolution of dissolved and particulate organic matter along the lower Amazon River-Óbidos to the ocean. *Marine Chemistry*, *177*, 244–256. https://doi.org/10.1016/j.marchem.2015.06.013

Watkins, M. M., Wiese, D. N., Yuan, D.-N., Boening, C., & Landerer, F. W. (2015). Improved methods for observing Earth's time variable mass distribution with GRACE using spherical cap masconsImproved methods for observing Earth's time variable mass distribution with GRACE using spherical cap mascons. *Journal of Geophysical Research: Solid Earth*, *120*(4), 2648–2671. https://doi.org/10.1002/2014JB011547

Watkins, M. M., & Yuan, D.-N. (2014). *GRACE gravity Recovery and climate experiment JPL Level-2 processing standards document for level-2 product Release 05.1*.

Wu, H., Kimball, J. S., Mantua, N., & Stanford, J. (2011). Automated upscaling of river networks for macroscale hydrological modeling. *Water Resources Research*, *47*(3). https://doi.org/10.1029/2009WR008871

Yang, Z., & Dominguez, F. (2019). Investigating land surface effects on the moisture transport over South America with a moisture tagging model. *Journal of Climate*, *32*(19), 6627–6644.Retrieved from https://journals.ametsoc.org/view/journals/clim/32/19/jcli-d-18-0700.1.xml. https://doi.org/10.1175/JCLI-D-18-0700.1

Yilmaz, M. T., DelSole, T., & Houser, P. R. (2011). Improving land data assimilation performance with a water budget constraint. *Journal of Hydrometeorology*, *12*(5), 1040–1055. https://doi.org/10.1175/2011JHM1346.1

Zhang, Y., Pan, M., Sheffield, J., Siemann, A. L., Fisher, C. K., Liang, M., et al. (2018). A climate data record (CDR) for the global terrestrial water budget: 1984-2010. *Hydrology and Earth System Sciences*, *22*(1), 241–263. https://doi.org/10.5194/hess-22-241-2018

Zhang, Y., Pena Arancibia, J. L., McVicar, T. R., Chiew, F. H. S., Vaze, J., Chiangming, L., et al. (2016). Multi-decadal trends in global terrestrial evapotranspiration and its components. *Scientific Reports*. *6*(19124), https://doi.org/10.1038/srep19124